

# Passive Realizations of Series Elastic Actuation: Effects of Plant and Controller Dynamics on Haptic Rendering Performance

Celal Umut Kenanoglu

Volkan Patoglu

**Abstract**—We establish the necessary and sufficient conditions for the passivity of series (damped) elastic actuation (S(D)EA) while rendering Voigt models, linear springs, and the null impedance under velocity-sourced impedance control (VSIC). We introduce minimal passive physical equivalents for S(D)EA under closed-loop control to help establish an intuitive understanding of the passivity bounds and to highlight the effect of different plant parameters and controller gains on the closed-loop performance of the system. Through the passive physical equivalents, we rigorously compare the effect of different plant dynamics (e.g., SEA and SDEA) on the system performance. We demonstrate that passive physical equivalents make the effect of controllers explicit and establish a natural means for effective impedance analysis. We advocate for the co-design of S(D)EAs through simultaneous consideration of the controller and plant dynamics and demonstrate the usefulness of negative controller gains when used with properly designed plant dynamics. We provide experimental validations of our theoretical results and characterizations of the haptic rendering performance of S(D)EA under VSIC.

**Index Terms**—Physical human-robot interaction, interaction control, haptic rendering, series elastic actuation, network synthesis, passive physical realizations, coupled stability.

## I. INTRODUCTION

SAFE and natural physical human-robot interactions (pHRI) necessitate precise control of the impedance characteristics of the robot at the interaction port [1], [2]. Series elastic actuation (SEA) is a commonly employed interaction control paradigm that has been introduced in [3]–[5] to address the fundamental trade-off between the stability robustness and the control performance of closed-loop force control systems [6]–[9]. SEA relies on an intentionally introduced compliant element between the actuator and interaction ports and utilizes the model of this compliant element to implement closed-loop force control. Thanks to SEA, the strict stability bounds on the controller gains induced due to sensor-actuator non-collocation and bandwidth limitations can be relaxed, leading to high stability robustness and good rendering performance. On the negative side, the introduction of the compliant element significantly decreases the system bandwidth; consequently, the control effort increases quickly for high-frequency interactions, resulting in actuator (velocity and/or torque) saturation.

Series damped elastic actuation (SDEA) extends SEA by introducing a linear viscous dissipation element parallel to the series elastic element [10]–[14]. SDEA can, not only help increase the force control bandwidth of SEA [10] but also provide additional advantages, in terms of improving energy efficiency [12], reducing undesired oscillations [13], alleviating the need for derivative control terms [14], and relaxing the upper-bound on passively renderable stiffness [9].

Given S(D)EA is generally designed as lumped-parameter LTI systems, the coupled stability of interactions with S(D)EA has commonly been studied through passivity analyses. Since inanimate environments are passive and non-malicious human interactions do not intentionally aim to destabilize a system, the passivity analysis can be utilized to conclude coupled stability of pHRI [2]. While passivity conditions are known to be conservative, closed-form analytical passivity conditions derived through such analysis are informative, as they provide insights into how system parameters affect stability robustness.

**Contributions:** In this study, we rigorously study the passivity of S(D)EA to establish closed-form analytical solutions for the *necessary and sufficient conditions* for passivity of S(D)EA while rendering Voigt models, linear springs, and the null impedance. Our results significantly extend the previously established bounds in the literature, as we provide (i) passivity bounds for Voigt model rendering with S(D)EA under VSIC, (ii) establish the necessity and sufficiency of these conditions, and (iii) allow for the use of negative controller gains. Furthermore, we propose (iv) the use of *passive physical equivalents* as an informative means of providing physical insight into the passivity-performance trade-offs of S(D)EA, and (v) derive minimal passive physical equivalents for S(D)EA under closed-loop control. We advocate that passive physical equivalents are instrumental, as they

- provide sufficient conditions for the passivity bounds,
- establish an intuitive understanding of the passivity bounds by explicitly highlighting the contribution of each different plant parameter and controller gain on the closed-loop rendering performance,
- make the authority of controller terms on the plant parameters explicit,
- do not distinguish between the plant and controller parameters, promoting co-design of S(D)EA by enforcing simultaneous and unbiased consideration of these (possibly negative) parameters to improve system performance,
- subsume the effective impedance analysis that decom-

C. U. Kenanoglu is with the Munich Institute of Robotics and Machine Intelligence at Technical University of Munich, 80992, Germany. V. Patoglu is with the Faculty of Engineering and Natural Sciences at Sabancı University, İstanbul, 34956, Türkiye. C. U. Kenanoglu's work was carried out during his graduate studies at Sabancı University.  
E-mail: {umut.kenanoglu, volkan.patoglu}@sabanciuniv.edu

poses the output impedance into its basic mechanical primitives and extend it by providing a topological connection of these fundamental elements, and

- enable rigorous and intuitive comparisons of the effect of different plant/controller dynamics (e.g., SEA and SDEA) on the haptic rendering performance.

Our study not only establishes the feasibility of passive Voigt model rendering with SEA under VSIC through the use of negative controller gains but also demonstrates that such a control approach can be practicable through a co-design, where physical damping is intentionally added to the plant dynamics, for instance via electrical damping. It also provides the *necessary and sufficient conditions* for the passivity of S(D)EA while rendering Voigt models. Moreover, the derivation of minimal passive physical equivalents of S(D)EA that are close to the open-loop plant dynamics and that lend themselves to simple interpretations, ensuring continuity among various realizations utilizing different plant architectures, determination of the control authority of VSIC on plant parameters, and insightful discussions of effective impedance analysis via passive physical equivalents are among our novel contributions. Furthermore, our study provides a novel means of symbolic comparison among different plant/controller dynamics on system performance through minimal passive physical equivalents with continuity, allowing the designer to make informed decisions among various plants/controllers.

## II. RELATED WORK

### A. Passivity Analysis of SEA

Pratt *et al.* have presented the first passivity analysis for SEA, and provided sufficient conditions for a SEA under a filtered PID force controller with a feedforward compensator [4]. Since the introduction of velocity-sourced impedance control (VSIC) for SEA [3], [15]–[17], the passivity of SEA under VSIC has been studied extensively [9], [18]–[23]. VSIC has become the most popular force controller for SEA, as its cascaded control architecture with an inner motion control loop can effectively eliminate parasitic forces —undesired effects due to dissipation, compliance, inertial dynamics that negatively affect the rendering transparency, leading to a linear system and good rendering performance [3], [5], [17], [24]. Furthermore, VSIC is easy-to-use, since this controller does not rely on the dynamic model of the plant and the controller gains can be tuned empirically.

Vallery *et al.* have provided a set of sufficient conditions for null impedance and linear spring rendering with SEA under VSIC [18], [19]. They have also proved that the passively renderable stiffness of a SEA under VSIC is upper bounded by the physical stiffness of the compliant element of SEA [19]. Tagliamonte *et al.* have provided less conservative sufficient conditions for the passivity of SEA under VSIC during null impedance, linear stiffness, and Maxwell body rendering [20]. They have also proved that Voigt model *cannot* be passively rendered with SEA under VSIC when the controllers are PI-PI and the controller gains are positive. Calanca *et al.* have presented sufficient conditions for the passivity of SEA under four different control architectures: VSIC, basic impedance, collocated admittance, and collocated impedance controllers [21].

They have shown that the passively renderable virtual stiffness of all of these control architectures is also limited by the physical stiffness of the compliant element [21]. Calanca *et al.* have also advocated for the use of acceleration feedback to compensate for the load dynamics [21], [25]. While acceleration feedback can help improve performance [4], [5], [25], the fundamental passive stiffness rendering limitations of SEA cannot be relaxed by such a control effort, as long as the controllers are kept causal [9].

Tosun and Patoglu [22] have presented the necessary and sufficient conditions for the passivity of SEA under VSIC for null impedance and linear spring rendering. The earlier sufficiency bounds on controller gains have been relaxed and the range of impedances that can be passively rendered has been extended in this study. Furthermore, it has been shown that the integral gain of the motion controller is required to render stiffness if the force controller utilizes an integral term.

Authors have proposed the use of model reference force control (MRFC) for SEA and provided a passivity analysis of this control scheme, under model mismatch. In particular, sufficient conditions for the passivity of SEA under MRFC during null impedance rendering have been presented in [26].

Recently, authors have established a fundamental limitation of passive spring rendering with SEA, by proving that the physical stiffness of its compliant element cannot be exceeded with any (linear or nonlinear) causal controller [9]. Authors have also studied the effect of low-pass filtering on the passivity and rendering performance SEA under VSIC [23].

This study significantly extends the passivity results for SEA under VSIC in [9], [18]–[23] by deriving the necessary and sufficient conditions for the passivity of SEA under VSIC during Voigt model rendering. It establishes that passive rendering of Voigt models with SEA under VSIC is feasible when negative controller gains are utilized and demonstrates the practical application of such renderings through the addition of damping to the plant. This study also presents novel minimal passive physical equivalents of SEA under VSIC during the Voigt model, linear spring, and null impedance rendering.

### B. Passivity Analysis of SDEA

SDEA generalizes SEA by introducing a viscous dissipation element parallel to the series elastic element. Accordingly, the passivity analysis of SDEA also generalizes the passivity analysis of SEA. However, passivity analysis of SDEA has received relatively less attention in the literature, since the resulting closed-form solutions of these systems are more complex and much harder to interpret [11], [27]–[29].

The passive range of virtual stiffness and damping parameters for SDEA under a cascaded impedance controller with an inner torque loop acting on a velocity-compensated plant and load dynamics have been studied in [27]. In this controller, a positive velocity feedback loop provides velocity compensation by attempting to extend the bandwidth of the torque control loop under passivity constraints.

Oblak and Matjacic [11] have conducted a passivity analysis of SDEA under an unconventional basic impedance controller. In this controller, a force sensor is employed after the end-effector inertia to measure the interaction forces, and these

forces are used for closed-loop force control, in addition to the series damped elastic element. It has been demonstrated that a sufficient level of mechanical damping is required in the compliant element to ensure the passivity of linear stiffness rendering using this control architecture. Furthermore, sufficient conditions to passively render linear springs have been proposed, which include a lower bound on the required level of physical damping.

Mengilli *et al.* have presented sufficient conditions for the passivity of SDEA under VSIC for the null impedance, linear spring, and Voigt model rendering [29]. They have demonstrated that thanks to the damping of the compliant element, passive spring renderings with SDEA can exceed the physical stiffness of the compliant element. They have extended their results to absolute stability and two-port passivity analyses and derived the necessary and sufficient conditions for appropriate virtual couplers [28]. In [9], authors have studied the necessary and sufficient conditions for the passivity of linear spring rendering with SDEA under a cascaded controller that neglects the forces induced on the damping element.

This study significantly extends the one-port passivity results in [22] by extending them to SDEA, and the results in [9], [29] by establishing the necessity bounds for SDEA under VSIC and generalizing the results to include negative controller gains. This study also presents novel minimal passive physical equivalents of SDEA under VSIC to provide intuition about the passivity bounds and to study the trade-offs involved in the rendering performance.

### C. Realization of Passive Physical Equivalents

Passive physical equivalents are studied in the field of network synthesis, which aims to rigorously describe physically realizable behaviors in a given domain with specified components. Colgate and Hogan have advocated the use of passive physical equivalents for the analysis of contact instability observed in interaction control [30]. They have studied uncontrollable elements under all causal controllers and through passive mechanical realizations of force-controlled systems, they have demonstrated a fundamental limitation on inertia compensation under passivity constraints for force-feedback systems with sensor-actuator non-collocation. They have also illustrated that the passive physical equivalents promote the use of negative controller gains and a simultaneous consideration of the design of mechanical and controller subsystems.

Inspired by [30], this paper focuses on passive mechanical realizations of S(D)EA under VSIC. Extending the methods in [30], our linear passive mechanical networks are built utilizing springs, dampers, and *inerters*—a relatively recently introduced fundamental element of the mechanical domain [31], [32]. The use of the inerter element is crucial as it completes the force-current analogy between the electrical and mechanical domains by introducing an ideal linear two-terminal energy storage element equivalent to an ungrounded capacitor. The completion of the analogy has a major impact, as it enables all of the previously established results in the electrical network synthesis to be equivalently expressed in the mechanical domain. Thanks to this analogy, all classical results, including Foster’s reactance theorem [33] character-

izing lossless networks, Brune’s construction method [34] for the minimal realization of general positive-real functions using resistors, inductors, capacitors, and transformers, and Bott-Duffin theorem [35] indicating transformers are not necessary for the synthesis of positive-real impedances, can be directly used for the network synthesis in the mechanical domain.

While network synthesis in the electrical domain has received much attention during the era of analog circuits, the diminished attention has been renewed during the last decade, especially in the mechanical domain, with the introduction of inerter element and demonstration of its successful applications in the design of passive suspensions [31], [36]–[41].

Kalman has also advocated for a renewed focus on network synthesis to establish a general theory of the subject, pointing out the high potential of this field to have a wide impact in a broad range of applications [42]. Accordingly, recent results have been established to extend the classical ones. Chen and Smith have studied the most general class of mechanical impedances that can be realized using one damper, one inerter, and an arbitrary number of spring elements while allowing no levers [37]. Jiang and Smith have studied the realizability conditions for positive-real biquadratic impedance functions which can be realized by five-element [43] and six-element [44] networks. Chen *et al.* have extended their earlier results in [39] and established the realizability conditions to two special class of mechanical networks: networks with biquadratic functions with an extra pole at the origin [40] and networks that are constituted of one inerter, one damper, and at most three springs [41]. Hughes and Smith have extended the classical results on Bott–Duffin realization procedure by discussing the minimality and uniqueness of these realizations among all series-parallel networks realizing biquadratic minimum functions [45]. Hughes has further extended these results and established minimal network realizations for the class of impedances realized by series-parallel networks containing at most three energy storage elements [46]. Morelli and Smith have presented an enumerative approach to the passive network synthesis and provided a classification for networks of restricted complexity [47]. Readers are referred to the survey by Hughes *et al.* for a review of the recent developments [48].

To the best of the authors’ knowledge, this is the first study in which passive mechanical equivalents are systematically used to analyze passivity-performance trade-offs of S(D)EA. Furthermore, extending the methods utilized by the seminal work in [30], this study introduces inerter elements to the analysis of interaction control systems.

### D. Rendering Performance

While the coupled stability of pHRI systems constitutes an imperative design criterion, the rendering performance of the system is also significant for natural interactions. Transparency is a commonly used concept in the evaluation of the haptic rendering performance, as it quantifies the match between the mechanical impedance of the virtual environment and the impedance felt by the user, with the requirement of identical force/velocity responses [49], [50].  $Z_{\text{width}}$  is another commonly used metric that quantifies the difference between the minimum and the maximum passively renderable impedances [51].



Following useful lemmas have been established in the literature to determine the necessary and sufficient conditions for the passivity of LTI systems.

**Lemma 1.** Let  $Z(s) = N(s)/D(s)$  be an impedance transfer function. Then,  $\text{Re}[Z(jw)] \geq 0$  if and only if the test polynomial  $P(w) \geq 0$  for any value of  $w$ , where  $P(w) = \text{Re}[N(jw)D(-jw)] = \sum_{i=0}^n d_i w^i$ , and  $d_i$  represents the coefficient of  $w^i$ .

**Lemma 2.** Let  $f(s) = a_3 s^3 + a_2 s^2 + a_1 s + a_0$  for  $a_i \geq 0$  be the third-order characteristic equation of a system. Then,  $f(s)$  has no roots in the open right half plane if and only if  $a_3 \geq 0$ ,  $a_2 \geq 0$ ,  $a_0 \geq 0$ , and  $a_1 a_2 - a_0 a_3 \geq 0$ . If these inequalities are strictly greater than zero, then the system has no roots on the imaginary axis.

**Lemma 3** ([28]). A polynomial of the form  $p(x) = p_2 x^2 + p_1 x + p_0$ ,  $p(x) \geq 0$  for all  $x \geq 0$  if and only if  $p_2 \geq 0$ ,  $p_0 \geq 0$  and  $p_1 \geq -2\sqrt{p_0 p_2}$ .

### C. Passive Physical Equivalents and Inerter

**Definition 1.** Passive physical equivalents describe physically realizable behaviors with a passive network of fundamental elements in a domain to realize a driving-point impedance.

In the force-current analogy between the mechanical and electrical domains, forces are considered to be analogous to currents, while velocities are analogous to voltages. Passive mechanical networks are built utilizing springs, dampers, and inerters. The inerter is an ideal energy storage element that completes the force-current analogy between the mechanical and electrical domains [31], [32]. The inerter element generalizes the more familiar mass/inertia element in the mechanical domain, which is analogous to the restricted case of a grounded capacitor in the electrical domain.

**Definition 2.** An inerter is an ideal linear two-terminal energy storage element in the mechanical domain with terminal forces proportional to the relative acceleration between them.

Figure 3 presents the force-current analogy between fundamental two-terminal elements in both domains.

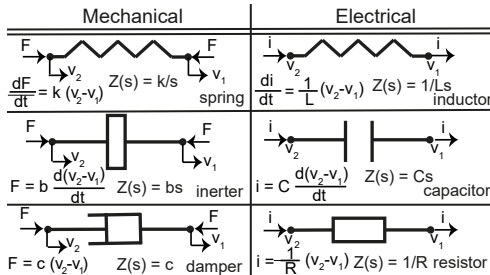


Fig. 3: Force-current analogy between the fundamental two-terminal elements in the electrical and mechanical domains.

## IV. PASSIVITY AND PHYSICAL EQUIVALENTS OF SDEA AND SEA UNDER VSIC

In this section, we present the necessary and sufficient conditions for the passivity of SDEA and SEA under VSIC with proportional (P) controllers while rendering Voigt, linear

spring, and null impedance models, without imposing a non-negativity assumption on the controller gains. Please note that the inner motion control loop is considered asymptotically stable throughout the analyses, imposing  $(B_m + G_m) > 0$ .

### A. Voigt Model Rendering

In this subsection, we present the necessary and sufficient conditions for the passivity of S(D)EA under VSIC while rendering Voigt models. Furthermore, we present passive physical equivalents of S(D)EA during Voigt model rendering.

1) *Series Damped Elastic Actuation*: When both the torque and velocity controllers of VSIC are proportional, the impedance at the interaction port of SDEA under VSIC during Voigt model rendering is  $Z_{Voigt}^{SDEA^{P-P}}(s) =$

$$\frac{B_f J_m s^3 + [B_f(B_m + G_m) + J_m K + B_{ref} B_f \alpha] s^2 + [K(B_m + G_m + B_{ref} \alpha) + B_f K_{ref} \alpha] s + K K_{ref} \alpha}{J_m s^3 + [B_m + G_m + B_f(1 + \alpha)] s^2 + K(1 + \alpha) s} \quad (1)$$

where  $\alpha = G_m G_t$ . Theorem 2 presents the necessary and sufficient conditions for the passivity of SDEA under VSIC while rendering Voigt models.

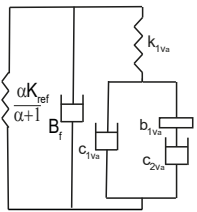
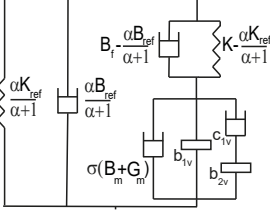
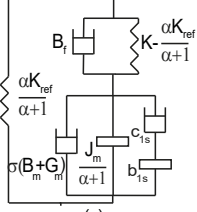
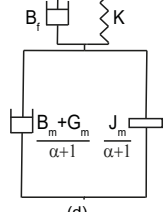
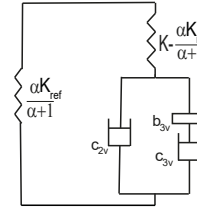
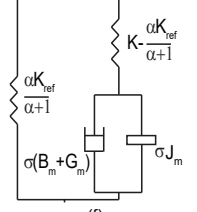
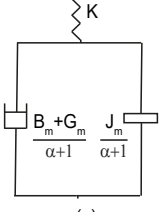
**Theorem 2.** Consider Voigt model rendering with SDEA under VSIC as in Figure 1, where the torque and velocity controllers consist of proportional gains  $G_t$  and  $G_m$ , respectively. Let the physical plant parameters be positive, while the controller gains are allowed to be negative as long as the inner motion control loop is asymptotically stable. Then, the following inequalities serve as the necessary and sufficient conditions for establishing the passivity of  $Z_{Voigt}^{SDEA^{P-P}}(s)$ :

- (i)  $0 < \frac{\alpha}{\alpha+1} K_{ref} \leq \left(1 + \frac{\alpha B_{ref}}{B_m + G_m}\right) K$ , and
- (ii)  $-(B_m + G_m) \leq \alpha B_{ref}$ , and
- (iii)  $0 < (\alpha + 1)$ , and
- (iv)  $0 < (B_m + G_m)$ , and
- (v)  $-2J_m \sqrt{B_f K} [(B_m + G_m + B_{ref} \alpha) K (\alpha + 1) - (B_m + G_m) K_{ref} \alpha] \leq B_f (B_m + G_m + B_{ref} \alpha) [B_m + G_m + B_f (\alpha + 1)] - (B_{ref} K + B_f K_{ref}) J_m \alpha$ .

*Proof:* First, note that asymptotic stability of the inner loop imposes  $(B_m + G_m) > 0$ . Next, according to Theorem 1;

- (1)  *$Z(s)$  has no poles in the right half plane*: Invoking Lemma 2 imposes  $(\alpha + 1)(B_m + G_m + B_f(\alpha + 1)) \geq 0$ . Accordingly,  $Z_{Voigt}^{SDEA^{P-P}}(s)$  has no roots in the open right half plane, if  $(\alpha + 1)$  and  $B_m + G_m + B_f(\alpha + 1)$  are non-negative.
- (2) *Any poles of  $Z(s)$  on the imaginary axis are simple with positive and real residues*: If  $(\alpha + 1)$  is positive, then only possible root on the imaginary axis is  $s = 0$  as long as physical parameters are positive and inner motion loop is asymptotically stable. For the pole at  $s = 0$ , the residue equals to  $\frac{\alpha}{(\alpha+1)} K_{ref}$  which should be positive. If  $(\alpha + 1) = 0$ , then the output impedance transfer function has double roots and Condition 3 of Theorem 1 is violated due to double poles at  $s = 0$ . Hence, when  $(\alpha + 1) = 0$ , passive Voigt models cannot be rendered.
- (3)  *$\text{Re}[Z(jw)] \geq 0$  for all  $w$* : The sign of  $\text{Re}[Z_{Voigt}^{SDEA^{P-P}}(jw)]$  can be checked by the sign of the test polynomial  $H(jw) = d_6 w^6 + d_4 w^4 + d_2 w^2$  from Lemma 1, where

TABLE I: Passive physical equivalents for SDEA and SEA under VSIC with P-P controllers

	Voigt Model Rendering		Spring Rendering	Null Impedance Rendering
	Negative $B_{ref}$	Positive $B_{ref}$		
SDEA				
SEA		No passive realization exists.		

$$d_2 = K^2 (\alpha+1) (B_m + G_m + B_{ref} \alpha) - (B_m + G_m) K K_{ref} \alpha \quad (2)$$

$$d_4 = B_f (B_m + G_m + B_{ref} \alpha) [B_m + G_m + B_f (\alpha+1)] - (B_{ref} K + B_f K_{ref}) J_m \alpha \quad (3)$$

$$d_6 = B_f J_m^2 \quad (4)$$

Applying Lemma 3, and noting that  $d_6$  is positive, since  $B_f$  is positive, the following constraint is imposed by the non-negativeness of  $d_2$ :

$$K \geq K_{ref} \frac{\alpha}{(\alpha+1)} \frac{B_m + G_m}{B_m + G_m + B_{ref} \alpha} \quad (5)$$

The last necessary and sufficient condition reads as:

$$\begin{aligned} -2 J_m \sqrt{B_f K [(B_m + G_m + B_{ref} \alpha) K (\alpha+1) - (B_m + G_m) K_{ref} \alpha]} \\ \leq B_f (B_m + G_m + B_{ref} \alpha) [B_m + G_m + B_f (\alpha+1)] - (B_{ref} K + B_f K_{ref}) J_m \alpha \end{aligned} \quad (6)$$

**Remark (1).** A (more conservative) set of sufficient conditions can be derived by considering Conditions (i)–(iv) together with the following inequality instead of Condition (v):

$$J_m \leq \frac{B_f (B_m + G_m + B_{ref} \alpha) [B_m + G_m + B_f (1+\alpha)]}{(B_f K_{ref} + B_{ref} K) \alpha} \quad (7)$$

**Passive Physical Equivalent of SDEA under VSIC:** A minimal realization of Eqn. (1) characterizing SDEA under VSIC during Voigt model rendering when both controllers are P and  $B_{ref} > 0$  is presented in Table Ib, where the parameters of this physical realization can be listed as

$$\begin{aligned} b_{1v} &= \frac{J_m}{(\alpha+1)^2} - \frac{\alpha}{(\alpha+1)^2} \frac{(B_{ref} - B_f)}{B_f} J_m \\ c_{1v} &= \frac{\alpha}{(\alpha+1)^2} \frac{(B_f K_{ref} - B_{ref} K) [B_f (B_m + G_m) - J_m K]}{B_f^2 K} \\ b_{2v} &= \frac{\alpha}{(\alpha+1)^2} \frac{(B_f K_{ref} - B_{ref} K) [B_f (B_m + G_m) - J_m K]}{B_f K^2} \end{aligned}$$

$$\text{with } \sigma = \frac{1}{\alpha+1} - \frac{\alpha}{(\alpha+1)^2} \frac{K_{ref}}{K}.$$

For the realization in Table Ib to be feasible, all components of the model should be non-negative. First of all,  $\frac{\alpha}{\alpha+1} B_{ref}$  and  $\frac{\alpha}{\alpha+1} K_{ref}$  should be positive to have a feasible realization in Table Ib while rendering Voigt models. When  $G_m$  and  $G_t$  are non-negative, the non-negativeness of these terms imposes

$$K \geq \frac{\alpha}{\alpha+1} K_{ref} \quad (8)$$

$$B_f \geq \frac{\alpha}{\alpha+1} B_{ref} \quad (9)$$

$$\frac{B_f}{K} \geq \frac{J_m}{(B_m + G_m)} \quad (10)$$

Substituting Eqn. (9) into  $(B_f K_{ref} - B_{ref} K)$  and invoking Eqn. (8), one can prove that  $(B_f K_{ref} - B_{ref} K) \geq 0$ . Eqns. (8) and (9) impose the upper bounds on passively renderable stiffness and damping levels.

In Eqn. (10),  $\frac{J_m}{(B_m + G_m)}$  captures the time constant of the motion-controlled mass-damper system, while  $\frac{B_f}{K}$  is the time constant of the serial physical filter. Accordingly, the condition in Eqn. (10) imposes the intuitive constraint that the motion-controlled mass-damper model of the plant should respond faster than the interaction forces filtered by the physical filter, such that the system can keep up with these inputs to adequately cancel out the undesired dynamics and superpose the virtual impedance to be rendered.

Table Ia presents a minimal realization of Eqn. (1) characterizing SDEA under VSIC during Voigt model rendering when both controllers are P and  $B_{ref} < 0$ . This realization is presented as it, not only complements the realization in Table Ib for negative  $B_{ref}$  values but also ensures continuity with the realization of SEA under VSIC during Voigt model rendering. The elements of this realization are prohibitively more complicated and only analyzed in the next section for the relatively simpler case of SEA.

**Feasibility of Passive Realization vs Passivity:** The feasibility conditions in Eqns. (8)–(10) serve as a set of sufficient conditions for the passivity of SDEA under VSIC. In particular, Eqn. (8) is a more conservative condition than Condition (i) of Theorem 2 as shown below:

$$K \geq K_{ref} \frac{\alpha}{(\alpha+1)} \geq K_{ref} \frac{\alpha}{(\alpha+1)} \frac{B_m + G_m}{B_m + G_m + B_{ref} \alpha} \quad (11)$$

Similarly, Eqn. (10) imposes a constraint that is more conservative than the sufficiency condition in Eqn. (7), as can be shown by substituting Condition (i) of Theorem 2 into Eqn. (7) and noting that the plant parameters are positive.



$$J_m \leq \frac{B_f}{K} (B_m + G_m) \leq \frac{B_f (B_m + G_m + B_{ref} \alpha) [B_m + G_m + B_f (1 + \alpha)]}{(B_f K_{ref} + B_{ref} K) \alpha} \quad (12)$$

Consequently, the feasibility of the realization in Table Ib provides a set of sufficient conditions for the passivity of Eqn. (1). Accordingly, the realization in Table Ib is valid when Eqns. (8)–(10) are satisfied with positive  $\frac{\alpha}{\alpha+1} B_{ref}$  and  $\frac{\alpha}{\alpha+1} K_{ref}$  values.

**Haptic Rendering Performance:** The physical realization of SDEA under VSIC during Voigt model rendering in Table Ib indicates three main branches in parallel: a spring-damper pair  $\frac{\alpha}{(\alpha+1)} K_{ref} - \frac{\alpha}{(\alpha+1)} B_{ref}$  in parallel that converges to the Voigt model to be rendered, and a branch capturing the parasitic dynamics which are governed by a complex structure of damper-inertance terms that is connected to the system through a coupling filter that operates in series.

The coupling filter consists of a spring-damper pair in parallel, where the stiffness and damping of the filter are given by  $K - \frac{\alpha}{(\alpha+1)} K_{ref}$  and  $B_f - \frac{\alpha}{(\alpha+1)} B_{ref}$ , respectively. The coupling filter indicates that the parasitic dynamics become more decoupled from the system as the control gains  $G_t$  and  $G_m$  increase. Furthermore, given that the coupling filter terms need to be positive, upper bounds are imposed on  $K_{ref}$  and  $B_{ref}$  of the Voigt models that can be passively rendered.

The parasitic dissipation effects are split into two parts: a damper term scaled by  $\sigma = \frac{1}{\alpha+1} - \frac{\alpha}{(\alpha+1)^2} \frac{K_{ref}}{K}$  indicating a significant effect of the force control gain  $G_t$  on this damper term, and a series damper-inerter term that introduces frequency-dependent dissipation that increases with frequency. The parasitic inertance term is scaled by the factor  $\frac{1}{(\alpha+1)^2} - \frac{\alpha}{(\alpha+1)^2} \frac{(B_{ref} - B_f)}{B_f}$ , indicating that both control gains  $G_m$  and  $G_t$  have an equal effect on this inerter term.

**Effective Impedance Analysis:** Further understanding of system dynamics can be obtained by studying the effective impedance of an implementation [26], [53]. Effective impedance definitions decompose the frequency-dependent impedance function into its fundamental components, where the real positive part is associated with the effective damping, while the imaginary part is assigned to the effective spring and effective inertia based on their phase characteristics. The effective impedance analysis of the realization in Table Ib, after removing the rendered Voigt model  $\frac{\alpha}{(\alpha+1)} K_{ref} - \frac{\alpha}{(\alpha+1)} B_{ref}$  and the serial coupling filter  $(B_f - \frac{\alpha}{(\alpha+1)} B_{ref}) - (K - \frac{\alpha}{(\alpha+1)} K_{ref})$  pairs, indicates that the effective damping of the parasitic dynamics can be computed as

$$c_{effVoigt}^{SDEA}(\omega) = \frac{[B_f^2 [(B_m + G_m)(1 + \alpha)] - B_{ref} B_f \alpha (B_m + G_m) + J_m \alpha (B_{ref} K - B_f K_{ref})] \omega^2 + K (B_m + G_m) [K + \alpha (K - K_{ref})]}{B_f^2 (\alpha + 1)^2 \omega^2 + K^2 (\alpha + 1)^2} \quad (13)$$

Eqn. (13) converges to  $\sigma(B_m + G_m)$  at low frequencies, while it approaches to  $\sigma(B_m + G_m) + c_{1v}$  at high frequencies.

Similarly, one can compute the effective inertance of the parasitic dynamics as

$$b_{effVoigt}^{SDEA}(\omega) = \frac{B_f [B_f J_m - \alpha J_m (B_{ref} - B_f)] \omega^2 + J_m K^2 (1 + \alpha) + \alpha (B_f K_{ref} - B_{ref} K) (B_m + G_m) - J_m K K_{ref} \alpha}{B_f^2 (\alpha + 1)^2 \omega^2 + K^2 (\alpha + 1)^2} \quad (14)$$

At the low frequency range, Equation (14) converges to  $b_{1v} + b_{2v}$ , whereas at the high frequency range, it approaches to  $b_{1v}$ . Accordingly, the parasitic damping of  $\sigma(B_m + G_m)$  affects the Voigt model rendering performance at the low frequency range, while a parasitic inertance of  $b_{1v} + b_{2v}$  is also effective in this frequency range. The force controller  $G_t$  can effectively mitigate the parasitic damping at low frequencies. The effective parasitic damping increases with frequency and  $c_{1v}$  is added to  $\sigma(B_m + G_m)$  at the high frequency range. On the other hand, the effective parasitic inertance decreases with frequency, and  $b_{1v}$  becomes more dominant at high frequencies. Hence, the effect of inertance at the low frequency range can be attenuated by both  $G_t$  and  $G_m$  gains.

Note that, for large controller gains  $G_t$  and  $G_m$ , the dynamics of the parasitic impedance becomes more decoupled from the rendered impedance  $\frac{\alpha}{(\alpha+1)} K_{ref} - \frac{\alpha}{(\alpha+1)} B_{ref}$  through the serial coupling filter. Furthermore, the rendered impedance converges to the desired Voigt model.

**2) Series Elastic Actuation:** When the torque and the motion controllers are proportional, the impedance at the interaction port of SEA under VSIC during Voigt rendering is  $Z_{Voigt}^{SEAP-P}(s) =$

$$\frac{J_m K s^2 + (B_m K + G_m K + B_{ref} K \alpha) s + K K_{ref} \alpha}{J_m s^3 + (B_m + G_m) s^2 + (K + K \alpha) s} \quad (15)$$

Corollary 1 presents the necessary and sufficient conditions for the passivity of SEA under VSIC while rendering Voigt models.

**Corollary 1.** Consider Voigt model rendering with SEA under VSIC as in Figure 1 with  $B_f=0$ , where the torque and velocity controllers consist of proportional gains  $G_t$  and  $G_m$ , respectively. Let the plant parameters be positive, while the controller gains are allowed to be negative as long as the inner motion control loop is asymptotically stable. Then, the following inequalities serve as the necessary and sufficient conditions for establishing the passivity of  $Z_{Voigt}^{SEAP-P}(s)$ :

- (i)  $0 < \frac{\alpha}{\alpha+1} K_{ref} \leq \left(1 + \frac{\alpha B_{ref}}{B_m + G_m}\right) K$ , and
- (ii)  $-(B_m + G_m) \leq \alpha B_{ref} \leq 0$ , and
- (iii)  $0 < (\alpha + 1)$ , and
- (iv)  $0 < (B_m + G_m)$ .

The proof follows from Theorem 2 by substituting  $B_f = 0$ . Please note that Corollary 1 indicates that  $B_{ref}$  and  $\alpha$  should have opposite signs.

**Passive Physical Equivalent:** A realization of Eqn. (15) characterizing SEA under VSIC during Voigt model rendering when both controllers are P is presented in Table Ie. The parameters of this realization include  $c_{2v} = \frac{B_m + G_m + B_{ref} \alpha}{\alpha + 1} - \frac{\alpha K_{ref} (B_m + G_m)}{K (\alpha + 1)^2}$ . The rest of the terms are relatively long and complicated; hence, they are presented as a Matlab script that allows for a numerical means of checking for the non-

negativeness of each element<sup>1</sup>.

**Feasibility of Passive Realization vs Passivity:** If we consider  $G_m$  and  $G_t$  to be non-negative, then symbolic substitutions and numerical evaluations indicate that the non-negativeness of  $c_{2v}$  imposes Condition (i) of Corollary 1. Moreover, if we substitute the non-negativeness condition of  $c_{2v}$  into  $b_{3v}$  and  $c_{3v}$ , we observe that  $B_{ref}$  should be negative for non-negativeness of  $b_{3v}$  and  $c_{3v}$ . Hence, the feasibility of the realization in Table Ie provides sufficient conditions for the passivity of the system. Accordingly, if we consider that the controller gains are positive, then the realization in Table Ie is valid as long as  $B_{ref}$  is negative, and Condition (i) of Corollary 1 are satisfied with non-negative  $b_{3v}$  and  $c_{3v}$  values.

The Voigt model rendering realization for SEA presented in Table Ie is valid only for the negative values of  $B_{ref}$ , as positive values of  $B_{ref}$  do not result in passive Voigt model rendering for SEA under VSIC with P-P controllers. The realization in Table Ie can be recovered from the SDEA realization in Table Ia, when  $B_f$  is set to zero. On the other hand, the realizations in Table Ib and Table Ie have distinct topology as they cover non-overlapping system parameters.

**Haptic Rendering Performance:** The physical realization of SEA under VSIC during Voigt model rendering in Table Ie indicates two main branches in parallel: a spring and a branch capturing the dynamics governed by a topology of damper-inertance terms that are coupled to the system through a spring in series. The parallel spring  $\frac{\alpha}{(\alpha+1)} K_{ref}$  indicates that, SEA can render the desired spring levels as the dominant behavior of the output impedance function in the low-frequency range.

Furthermore, in the realization presented in Table Ie, both damping elements  $c_{2v}$  and  $c_{3v}$  are functions of  $B_{ref}$ . Since  $c_{2v}$  is more dominant than  $c_{3v}$  in the low-frequency range, it can be concluded that  $c_{2v}$  mainly contributes to the rendered damping, while the effect of  $c_{3v}$  is added to  $c_{2v}$  as the frequency increases.

When a high value of  $G_t$  is selected,  $c_{2v}$  approaches  $B_{ref}$  at low frequencies, indicating that the damping in the system approaches to  $B_{ref}$ . However, please note that passivity of the system dictates that  $B_{ref}$  should be negative, while feasibility of the realization necessitates that  $c_{2v}$  cannot be negative. Accordingly, the realization becomes infeasible before  $c_{2v}$  can converge to  $B_{ref}$ . Similarly, as  $G_t$  increases, the total damping in the system approaches to zero. Finally,  $b_{3v}$  acts as a frequency-dependent parasitic inertance term because of its serial connection with  $c_{2v}$ .

The coupling filter consists of  $K - \frac{\alpha}{(\alpha+1)} K_{ref}$ , indicating that  $c_{2v}$  and  $c_{3v}$  become more coupled with the rest for the system with the lower choices of  $K_{ref}$ . This also implies that pure damping can be rendered at the lower frequency range with the selection of low  $K_{ref}$  values.

Please note that the maximum damping that can be passively rendered with SEA under VSIC during Voigt model rendering is upper bounded by  $\frac{B_m+G_m}{\alpha+1}$  and lower bounded by zero. Hence, the plant damping  $B_m$  and the VSIC controller gains

$G_t$  and  $G_m$  dictate the damping upper bound, while the (negative)  $B_{ref}$  acts as a control parameter that adjusts the amount of damping compensation in the system during Voigt model rendering.

**Effective Impedance Analysis:** To analyze the effective impedance of the realization in Table Ie, the effective damping and inertance are computed after removing the rendered virtual stiffness  $\frac{\alpha}{(\alpha+1)} K_{ref}$  and the serial coupling filter  $K - \frac{\alpha}{(\alpha+1)} K_{ref}$  from the system. The computed effective damping converges to  $c_{2v}$  at low frequencies, while it approaches to  $c_{2v}+c_{3v}$  at high frequencies. Similarly, the effective inertance converges to  $b_{3v}$  at low frequencies, while it approaches zero at high frequencies. Therefore,  $c_{2v}$  is the dominant damping in the low-frequency range, and  $c_{3v}$  is added to  $c_{2v}$  as the frequency increases. While the parasitic effect of  $b_{3v}$  exists in low frequencies, this effect will not be dominant in this frequency range, since the branch including  $c_{2v}$  is more dominant than serial  $c_{3v}$ - $b_{3v}$  pair. Due to their serial connection, the effect of  $b_{3v}$  becomes higher as the frequency increases, but at the same time, effective inertance goes to zero at high frequencies.

## B. Spring Rendering

In this subsection, we present the necessary and sufficient conditions for the passivity of S(D)EA under VSIC while rendering linear springs. Furthermore, we present passive physical equivalents of S(D)EA during linear spring rendering.

**1) Series Damped Elastic Actuation:** When the torque and the motion controllers are proportional, the impedance at the interaction port of SDEA under VSIC during linear spring rendering equals to

$$Z_{spring}^{SDEA^{P-P}}(s) = \frac{B_f J_m s^3 + (B_f (B_m + G_m) + J_m K) s^2 + (K (B_m + G_m) + B_f K_{ref} \alpha) s + K K_{ref} \alpha}{J_m s^3 + (B_f (1 + \alpha) + B_m + G_m) s^2 + K(\alpha + 1) s} \quad (16)$$

Corollary 2 presents the necessary and sufficient conditions for the passivity of SDEA under VSIC while rendering springs.

**Corollary 2.** Consider spring rendering with SDEA under VSIC as in Figure 1, where the torque and velocity controllers consist of proportional gains  $G_t$  and  $G_m$ , respectively. Let the physical plant parameters be positive, while the controller gains are allowed to be negative as long as the inner motion control loop is asymptotically stable. Then, the following expressions constitute the necessary and sufficient conditions for the passivity of  $Z_{spring}^{SDEA^{P-P}}(s)$ :

- (i)  $0 < \frac{\alpha}{\alpha+1} K_{ref} \leq K$ , and
- (ii)  $0 < (\alpha + 1)$ , and
- (iii)  $0 < (B_m + G_m)$ , and
- (iv)  $-2 J_m \sqrt{B_f K (B_m + G_m) (K + \alpha (K - K_{ref}))} \leq B_f ((B_m + G_m) (B_f (1 + \alpha) + B_m + G_m) - \alpha J_m K_{ref})$ .

The proof follows from Theorem 2 after substituting  $B_{ref} = 0$ .

**Passive Physical Equivalent:** A minimal realization of Eqn. (16) characterizing SDEA under VSIC during spring rendering when both controllers are P is presented in Table Ic, where  $c_{1s} = \frac{K_{ref} \alpha (B_f (B_m + G_m) - J_m K)}{B_f K (\alpha + 1)^2}$ ,  $b_{1s} = \frac{K_{ref} \alpha (B_f (B_m + G_m) - J_m K)}{K^2 (\alpha + 1)^2}$ , and  $\sigma = \frac{1}{\alpha + 1} - \frac{\alpha}{(\alpha + 1)^2} \frac{K_{ref}}{K}$ .

<sup>1</sup>The Matlab script that presents the parameters of the realization in Table Ie is available for download at [https://hmi.sabanciuniv.edu/SEA\\_Voigt-Realization.m](https://hmi.sabanciuniv.edu/SEA_Voigt-Realization.m).



For the realization in Table Ic to be feasible, all physical components of the model should be non-negative. Hence,  $(\alpha + 1)$  should be positive. Furthermore, the non-negativeness of the coupling spring imposes Condition (i) of Corollary 2. The non-negativeness  $\sigma(B_m + G_m)$  is guaranteed if  $(B_m + G_m) > 0$  and Condition (i) of Corollary 2 are simultaneously satisfied. The virtual stiffness is rendered as  $\frac{\alpha}{\alpha+1} K_{ref}$ . The conditions for the non-negativeness of  $c_{1s}$  and  $b_{1s}$  can be derived as

$$J_m \frac{K}{B_f} \leq (B_m + G_m) \quad (17)$$

which indicates  $(B_m + G_m) > 0$ .

**Feasibility of Passive Realization vs Passivity:** The feasibility conditions for the realization in Table Ic provide sufficient conditions for the passivity of Eqn. (16). This can be shown by first considering a sufficient condition for the passivity that is ensured by imposing a non-negative value to the intermediate coefficient of the test polynomial as follows

$$J_m \leq \frac{(B_m + G_m)(B_m + G_m + B_f(\alpha + 1))}{\alpha K_{ref}} \quad (18)$$

Note that replacing the condition provided in Condition (iv) of Corollary 2 with the non-negativeness of the intermediate coefficient of the test polynomial provides a (more conservative) sufficient condition for the passivity. This condition still needs to be considered together with the other necessary conditions of the non-negativeness of the highest and lowest coefficients of the test polynomial. Eqns. (17) and (18) can be arranged together as

$$J_m \leq \frac{(B_m + G_m) B_f}{K} \leq \frac{(B_m + G_m)(B_m + G_m + B_f(\alpha + 1))}{\alpha K_{ref}} \quad (19)$$

Given Condition (i) of Corollary 2 as necessitated by the feasibility of the realization in Table Ic and the passivity of Eqn. (16), this inequality is always satisfied. Therefore, Eqn. (17) is a more conservative sufficient condition than the one provided in Eqn. (18) and when Eqn. (17) is satisfied, Condition (iv) of Corollary 2 is guaranteed to hold.

Accordingly, the realization in Table Ic is feasible and valid and the sufficient conditions for the passivity of Eqn. (16) are satisfied if  $(B_m + G_m)$ ,  $(\alpha + 1)$ , and  $\frac{\alpha}{\alpha+1} K_{ref}$  are positive, and Eqn. (17) is satisfied. If Condition (iv) of Corollary 2 is replaced with Eqn. (17), then the necessary and sufficient conditions for the passivity of Eqn. (16) can be recovered.

**Haptic Rendering Performance:** The physical realization of SDEA during linear spring rendering in Table Ih indicates two branches in parallel: an ideal spring  $\frac{\alpha}{\alpha+1} K_{ref}$  whose stiffness approaches to  $K_{ref}$  as the controller gains get large and parasitic dynamics governed by damper-inertance elements that are serially coupled to the system with a spring-damper pair  $\left(K - \frac{\alpha}{\alpha+1} K_{ref}\right) - B_f$  in parallel.

Due to the existence of the physical filter damping  $B_f$  in parallel to the coupling spring, the parasitic dynamics cannot be completely decoupled from the system as the controller gains  $G_t$  and  $G_m$  increase, since  $B_f$  term dominates the coupling at the intermediate and high frequencies. Table Ih indicates that the parasitic effects of the damper  $\sigma(B_m + G_m)$

and the inerter  $J_m/(\alpha + 1)$  terms decrease with the choice of high controller gains. In particular,  $G_t$  has a more dominant effect on the damper term, while  $G_m$  and  $G_t$  gains affect the inerter term in the same manner, as they are multiplicative. In addition to these parallel damper-inerter terms, SDEA realization includes frequency-dependent dissipative effect which consists of serial damper-inerter terms.

**Effective Impedance Analysis:** An effective impedance analysis of the parasitic dynamics of the realization in Table Ic indicates that the effective damping of Eqn. (16) after removing the serial coupling filter  $B_f - \left(K - \frac{\alpha}{\alpha+1} K_{ref}\right)$  pair and the rendered stiffness  $\frac{\alpha}{\alpha+1} K_{ref}$  can be computed as

$$c_{effPP}^{SDEA} = \frac{B_f (B_f (B_m + G_m)(\alpha + 1) - J_m K_{ref} \alpha) \omega^2 + K (K (B_m + G_m)(\alpha + 1) - K_{ref} \alpha (B_m + G_m))}{B_f^2 (\alpha + 1)^2 \omega^2 + K^2 (\alpha + 1)^2} \quad (20)$$

At low frequencies, Eqn. (20) converges to  $\sigma(B_m + G_m)$ , while at high frequencies, Eqn. (20) approaches to  $\sigma(B_m + G_m) + c_{1s}$ . Similarly, the effective inertance for the parasitic dynamics of Eqn. (16) can be computed as

$$b_{effPP}^{SDEA} = \frac{(B_f^2 J_m (\alpha + 1)) \omega^2 + J_m K^2 (\alpha + 1) + B_f K_{ref} \alpha (B_m + G_m) - J_m K K_{ref} \alpha}{B_f^2 (\alpha + 1)^2 \omega^2 + K^2 (\alpha + 1)^2} \quad (21)$$

At low frequencies, Eqn. (21) converges to  $\frac{J_m}{\alpha+1} + b_{1s}$ , while at high frequencies, Eqn. (21) approaches to  $\frac{J_m}{\alpha+1}$ .

**2) Series Elastic Actuation:** When both the motion and torque controllers are proportional, the impedance at the interaction port of SEA under VSIC during spring rendering equals to

$$Z_{spring}^{SEA^{P-P}}(s) = \frac{J_m K s^2 + (B_m + G_m) K s + \alpha K K_{ref}}{J_m s^3 + (B_m + G_m) s^2 + (\alpha + 1) K s} \quad (22)$$

Corollary 3 presents the necessary and sufficient conditions for the passivity of SEA under VSIC while rendering springs.

**Corollary 3.** Consider spring rendering with SEA under VSIC as in Figure 1 with  $B_f = 0$ , where the torque and velocity controllers consist of proportional gains  $G_t$  and  $G_m$ , respectively. Let the physical plant parameters be positive, while the controller gains are allowed to be negative as long as the inner motion control loop is asymptotically stable. Then, the following expressions constitute the necessary and sufficient conditions for the passivity of  $Z_{spring}^{SEA^{P-P}}(s)$ :

- (i)  $0 < \frac{\alpha}{\alpha+1} K_{ref} \leq K$ , and
- (ii)  $0 < (\alpha + 1)$ , and
- (iii)  $0 < (B_m + G_m)$ .

The proof follows from Theorem 2 after substituting  $B_{ref} = 0$  and  $B_f = 0$ .

**Passive Physical Equivalent:** A minimal realization of Eqn. (22) characterizing SEA under VSIC during spring rendering when both controllers are P is presented in Table If, where  $\sigma = \frac{1}{\alpha+1} - \frac{\alpha}{(\alpha+1)^2} \frac{K_{ref}}{K}$ .

For the realization in Table If to be physically feasible, all of the components of the model should be non-negative.

All components in the realization are guaranteed to be non-negative, if  $K \geq \frac{\alpha}{\alpha+1} K_{ref}$  is satisfied, and  $(B_m + G_m)$ ,  $\frac{\alpha}{\alpha+1} K_{ref}$ , and  $(\alpha + 1)$  are positive.

**Feasibility of Passive Realization vs Passivity:** The conditions for the feasibility of the realization in Table If are equivalent to the necessary and sufficient conditions for the passivity of Eqn. (22): if  $K \geq \frac{\alpha}{\alpha+1} K_{ref}$  is satisfied and  $(B_m + G_m)$ ,  $(\alpha + 1)$ , and  $\frac{\alpha}{\alpha+1} K_{ref}$  are positive, then Eqn. (22) is passive and all components in Table If are non-negative. Accordingly, the realization is valid as long as the system is passive.

**Haptic Rendering Performance:** The physical realization of SEA during linear spring rendering in Table If indicates two branches in parallel: an ideal spring  $\frac{\alpha}{(\alpha+1)} K_{ref}$  whose stiffness approaches to  $K_{ref}$  as the controller gains get large and parasitic dynamics governed by a damper-inertance pair in parallel that is coupled to the system with a spring in series. The stiffness of the coupling spring is given by  $K - \frac{\alpha}{(\alpha+1)} K_{ref}$ ; hence, the parasitic dynamics get more decoupled from the system as the controller gains  $G_t$  and  $G_m$  increase. Note that, since the coupling spring needs to be positive for feasibility, this spring imposes an upper bound on  $K_{ref}$  that can be passively rendered. The parasitic damper-inertance dynamics is scaled by  $\sigma = \frac{1}{\alpha+1} - \frac{\alpha}{(\alpha+1)^2} \frac{K_{ref}}{K}$ , indicating that  $G_t$  has a significant effect for damper term, while both  $G_m$  and  $G_t$  equally affect the inerter term. Furthermore, the parasitic dynamics decrease with the choice of higher  $K_{ref}$  values. When  $K_{ref} = 0$ , the parasitic dynamics converge to that of null impedance rendering.

**Effective Impedance Analysis** The effective impedance of the system dynamics after the serial physical filter  $K - \frac{\alpha}{(\alpha+1)} K_{ref}$  and rendered stiffness  $\frac{\alpha}{(\alpha+1)} K_{ref}$  are extracted, is dominated by the damper term  $\sigma(B_m + G_m)$  in the low frequency range. Therefore, the spring rendering performance can be increased in the low frequency range by attenuating the effects of this damper term. Similarly, the high frequency behavior of these parasitic dynamics is dictated by the inerter term  $\sigma J_m$ .

### C. Null Impedance Rendering

In this subsection, we present the necessary and sufficient conditions for the passivity of S(D)EA under VSIC while rendering null impedance. We also present passive physical equivalents of S(D)EA during null impedance rendering.

1) *Series Damped Elastic Actuation:* When the torque and the motion controllers are proportional, the impedance at the interaction port of SDEA under VSIC during null impedance rendering equals to

$$Z_{null}^{SDEA^{P-P}}(s) = \frac{B_f J_m s^2 + (B_f (B_m + G_m) + J_m K) s + K(B_m + G_m)}{J_m s^2 + (B_f (1 + \alpha) + B_m + G_m) s + K(\alpha + 1)} \quad (23)$$

Corollary 4 presents the necessary and sufficient conditions for the passivity of SDEA under VSIC while rendering null impedance.

**Corollary 4.** Consider null impedance rendering with SDEA under VSIC as in Figure 1, where the torque and velocity

controllers consist of proportional gains  $G_t$  and  $G_m$ , respectively. Let the physical plant parameters be positive, while the controller gains are allowed to be negative as long as the inner motion control loop is asymptotically stable. Then, the following expressions constitute the necessary and sufficient conditions for the passivity of  $Z_{null}^{SDEA^{P-P}}(s)$ :

- (i)  $0 < (\alpha + 1)$ , and
- (ii)  $0 < (B_m + G_m)$ .

The proof follows from Theorem 2 after substituting  $B_{ref} = 0$  and  $K_{ref} = 0$ . Please note that when  $(\alpha + 1) = 0$ , the output impedance transfer function becomes  $B_f + \frac{K}{s}$ , which is passive but does not include a controllable virtual stiffness.

**Passive Physical Equivalent:** A minimal realization of Eqn. (23) characterizing SDEA under VSIC during null impedance rendering when both controllers are P is presented in Table Id. For the realization in Table Id to be feasible, all physical components in the model should be non-negative, which is guaranteed if  $(B_m + G_m)$  and  $(\alpha + 1)$  are positive.

**Feasibility of Passive Realization vs Passivity** The conditions for the feasibility of the realization in Table Id are equivalent to the necessary and sufficient conditions for the passivity of Eqn. (23): if  $(B_m + G_m) > 0$  and  $(\alpha + 1) > 0$ , then Eqn. (23) is passive and all components in Table Id are non-negative. Accordingly, the realization is valid as long as the system is passive.

**Haptic Rendering Performance:** Table Id indicates that the parasitic effect of the damper  $(B_m + G_m)/(\alpha + 1)$  and the inerter  $J_m/(\alpha + 1)$  terms decrease with the choice of high controller gains for SDEA during null impedance rendering.  $G_t$  has a more dominant effect on the damper term, while  $G_m$  and  $G_t$  gains affect the inerter term in the same manner, as their effects are multiplicative.

**Effective Impedance Analysis:** The effective impedance of the controllable part of the realization in Table Id, that is, the remaining system dynamics after the serial physical filter consisting of  $K - B_f$  terms is extracted, is dominated by the damper term  $(B_m + G_m)/(\alpha + 1)$  in the low frequency range. Therefore, the null impedance rendering performance can be increased in the low frequency range by attenuating the affects of this damper term. Similarly, the high frequency behavior of the parasitic dynamics is dictated by the inerter term  $J_m/(\alpha + 1)$ .

2) *Series Elastic Actuation:* When the torque and the motion controllers are proportional, the impedance at the interaction port of SEA under VSIC during null impedance rendering is

$$Z_{null}^{SEA^{P-P}}(s) = \frac{J_m K s + (B_m + G_m) K}{J_m s^2 + (B_m + G_m) s + (1 + \alpha) K} \quad (24)$$

Corollary 5 presents the necessary and sufficient conditions for the passivity of SEA under VSIC while rendering the null impedance.

**Corollary 5.** Consider null impedance rendering with SEA under VSIC as in Figure 1 with  $B_f = 0$ , where the torque and

velocity controllers consist of proportional gains  $G_t$  and  $G_m$ , respectively. Let the physical plant parameters be positive, while the controller gains are allowed to be negative as long as the inner motion control loop is asymptotically stable. Then, the following expressions constitute the necessary and sufficient conditions for the passivity of  $Z_{null}^{SEA^{P-P}}(s)$ :

- (i)  $0 < (\alpha + 1)$ , and
- (ii)  $0 < (B_m + G_m)$ .

The proof follows from Theorem 2 after substituting  $B_{ref} = 0$ ,  $K_{ref} = 0$ , and  $B_f = 0$ . Please note that when  $(\alpha + 1) = 0$ , the output impedance transfer function is  $\frac{K}{s}$ , which is passive but does not include a controllable virtual stiffness.

**Passive Physical Equivalent:** A minimal realization of Eqn. (24) characterizing SEA under VSIC during null impedance rendering when both controllers are P is presented in Table Ig. For the realization in Table Ig to be feasible, all physical components in the model should be non-negative, which is guaranteed if  $(B_m + G_m)$  and  $(\alpha + 1)$  are positive, given the plant parameters  $J_m$ ,  $B_m$ , and  $K$  are positive.

**Feasibility of Passive Realization vs Passivity:** The conditions for the feasibility of the realization in Table Ig are equivalent to the necessary and sufficient conditions for the passivity of Eqn. (24): if the  $(B_m + G_m) > 0$  and  $(\alpha + 1) > 0$ , then Eqn. (24) is passive and all components in Table Ig are non-negative. Accordingly, the realization is valid as long as the system is passive.

**Haptic Rendering Performance:** The physical realization of SEA under VSIC during null impedance rendering is identical to that of SDEA, except the fact that the physical filter of SEA does not include a physical damping term  $B_f$  parallel to the physical spring  $K$ . Similar to the case with SDEA, Table Ig indicates that the parasitic effect of the damper  $(B_m + G_m)/(\alpha + 1)$  and inerter  $J_m/(\alpha + 1)$  terms decrease with the choice of high controller gains for SEA during null impedance rendering. It can be observed from Table Ig that  $G_t$  has a more dominant effect on the damper term, while  $G_m$  and  $G_t$  gains affect the inerter term in the same manner, as their effects are multiplicative.

**Effective Impedance Analysis:** The effective impedance of the remaining system dynamics after the serial physical filter  $K$  is extracted is dominated by the damper term  $(B_m + G_m)/(\alpha + 1)$  in the low frequency range. Therefore, the null impedance rendering performance can be increased in the low frequency

range by attenuating the effects of this damper term. Similarly, the high frequency behavior of these parasitic dynamics is dictated by the inerter  $J_m/(\alpha + 1)$  term.

To summarize, the first row of Table I presents the passive mechanical realizations for SDEA under VSIC with P-P controllers, while the second row of Table I presents the passive mechanical realizations for SEA, while rendering Voigt, linear spring, and null impedance models. The minimal passive physical equivalents of S(D)EA are derived in such a way that their dynamics stay close to the open-loop plant dynamics to enable simple interpretations. Furthermore, continuity among the minimal passive physical equivalents is sought after to enable symbolic comparisons.

**Remark (2).** Table I indicates that there exists continuity among the realizations of both SDEA and SEA under VSIC; that is, by setting  $B_{ref} = 0$  in the realization of Voigt model rendering, the realization of spring rendering can be achieved. Similarly, the realization of null impedance rendering can be recovered from the realization of Voigt model rendering by setting  $B_{ref} = 0$  and  $K_{ref} = 0$ , simultaneously.

**Remark (3).** Table I also indicates that there exists continuity among the realizations of SDEA under VSIC and SEA under VSIC; that is, by setting  $B_f = 0$  in the SDEA realizations, the realizations of SEA can be recovered. Note that since the Voigt model rendering realization in Table Ib is valid only for the positive values of  $B_{ref}$ , while SEA under VSIC is not passive for  $B_{ref} > 0$ , no such realization exists for SEA. On the other hand, the realizations in Table Ia and Table Ie are both valid for  $B_{ref} < 0$  and display the desired continuity as their passive parameter ranges overlap.

## V. HAPTIC RENDERING PERFORMANCE

In this section, we study the effects of the physical plant parameters and the controller gains on the rendering performance through Bode plots. We also numerically evaluate the effective impedance of closed-loop systems. Only sample Bode plots in an order of increasing complexity are presented within the manuscript, for the brevity of discussion. The complete set of results is available in the Supplementary Document [61].

TABLE II: S(D)EA plant parameters used for the simulations

Parameter	$J_m$	$B_m$	$K$	$B_f$
Value	0.002 kg-m <sup>2</sup>	1.22 N-m s/rad	360 N-m/rad	0.5 N-m s/rad

Table II presents the physical parameters of the S(D)EA plant used in simulations to evaluate the system performance.

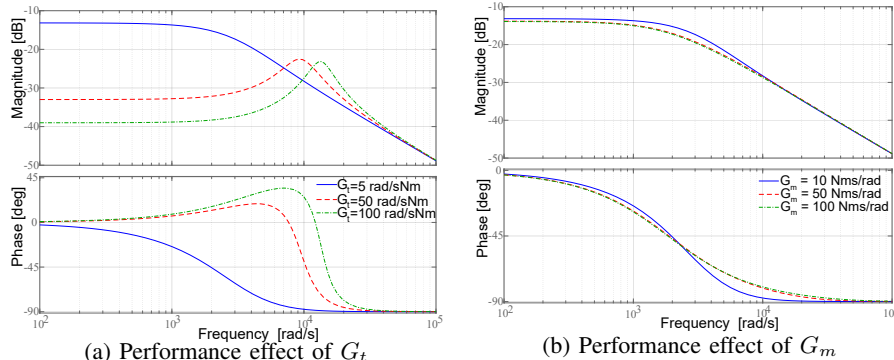
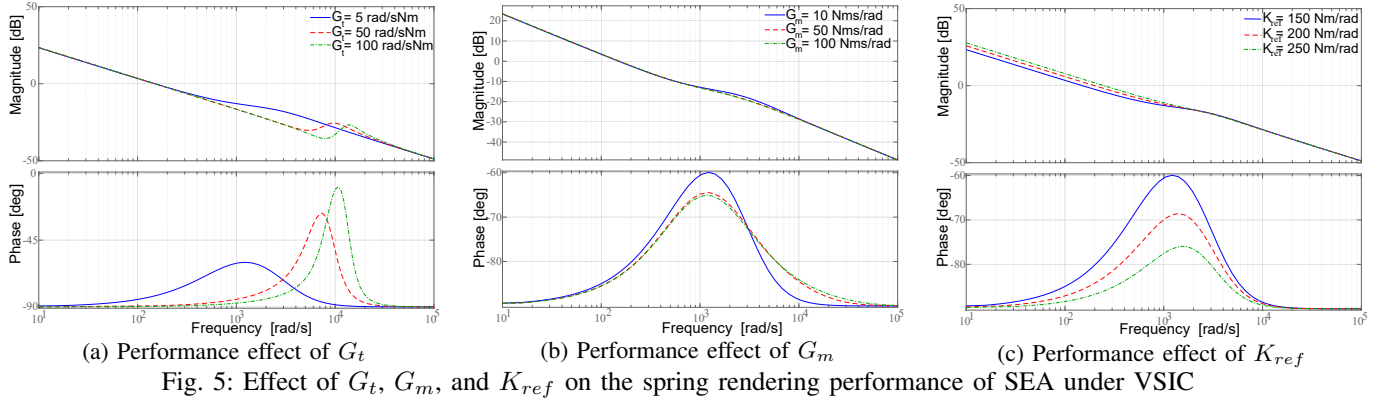


Fig. 4: Effect of  $G_t$  and  $G_m$  on the null impedance rendering performance of SEA under VSIC



The proportional controller gains are set as  $G_m = 10$  N-m s/rad and  $G_t = 5$  rad/(s N-m), respectively.

#### A. Effects of Controller Gains on Null Rendering Performance

**SEA:** Figure 4 presents the Bode plots depicting the performance of SEA under VSIC for various  $G_m$  and  $G_t$  controller gains. It can be observed from the Bode plots that the output impedance converges to the dynamics of the physical spring  $K$  at high frequencies and the controller gains shape this transition. Figure 4a indicates that the null impedance rendering performance can be significantly improved by employing higher  $G_t$  gains, leading to attenuated damping effects. Figure 4b shows that the effect of  $G_m$  gain is much less in the low frequency range. Figures 4a and 4b indicate that higher  $G_t$  and  $G_m$  gains enable smoother transitions from intermediate frequencies to high frequencies, reducing the resonant peak. The effects of controller gains on the null impedance rendering performance of SDEA are similar to the SEA case, presented in the Supplementary Document [61].

#### B. Effects of Controller Gains on Linear Spring Rendering

**SEA:** Since the high frequency dynamics of SEA are governed by the spring of its physical filter, all Bode plots converge to these dynamics. Figure 5a shows that, as the torque controller gain  $G_t$  is increased, the frequency range over which the virtual stiffness is successfully rendered can be significantly increased. Figures 5a and 5b indicate that, a smoother transition takes place at the intermediate frequency range to the spring of the physical filter at the high frequency range, when higher  $G_t$  gains are utilized. Similarly, Figure 5c shows that higher virtual stiffness levels can be rendered for higher  $K_{ref}$  selections, and as  $K_{ref}$  approaches  $K$ , the transition at the intermediate frequency range becomes smoother. Figure 5b indicates that higher  $G_m$  gains do not result in significant rendering performance differences at the low frequency range; however,  $G_m$  gains positively impact the disturbance response of the system, as shown in the next subsection. The effects of controller gains on the spring rendering performance of SDEA are similar to the SEA case.

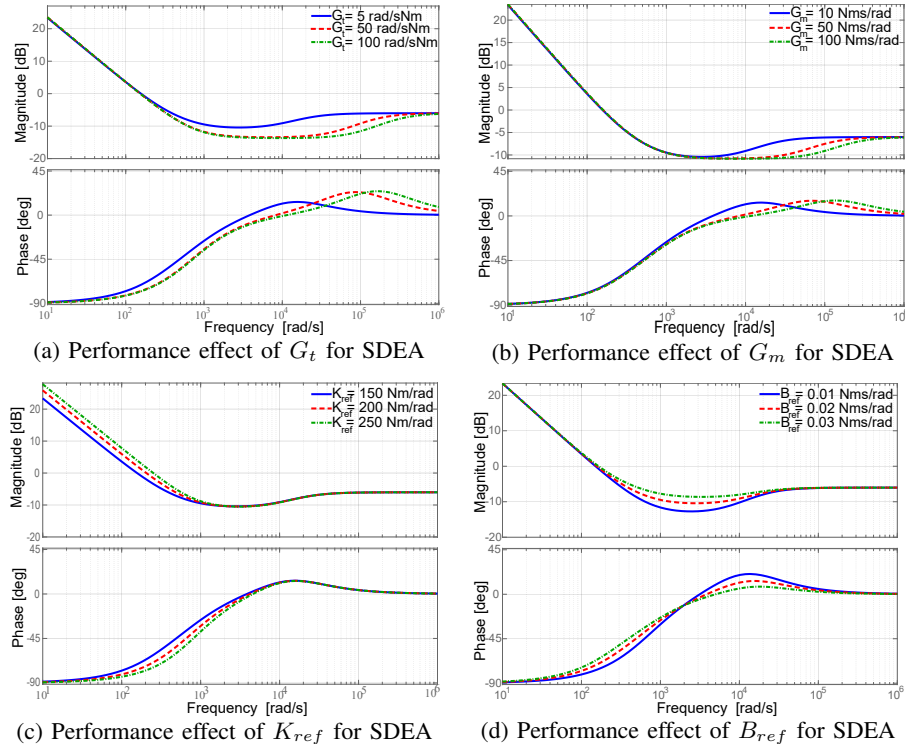


Fig. 6: Effect of  $G_t$ ,  $G_m$ ,  $K_{ref}$ , and  $B_{ref}$  on the Voigt model rendering performance of SDEA under VSIC

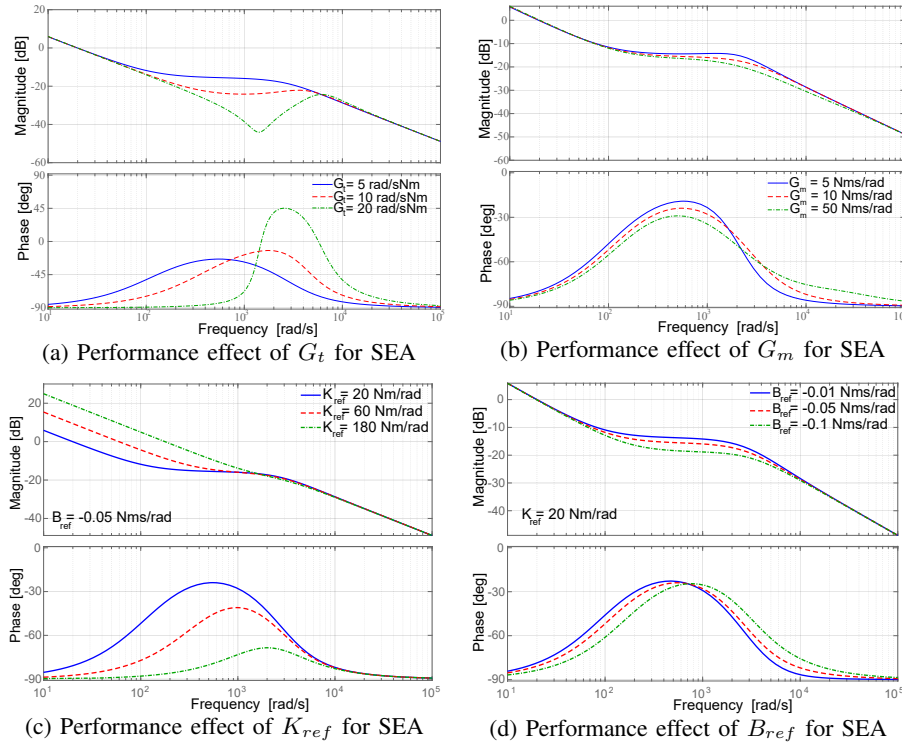


Fig. 7: Effect of  $G_t$ ,  $G_m$ ,  $K_{ref}$ , and  $B_{ref}$  on the Voigt model rendering performance of SEA under VSIC

### C. Effects of Controller Gains on Voigt Model Rendering

**SDEA:** Figure 6a demonstrates that an increase in  $G_t$  results in a wider frequency range for successful virtual stiffness and damping rendering. Figure 6b suggests that the changes in  $G_m$  have a minimal effect on spring rendering performance, but increase the range of virtual damping rendering as it results in a lower inerter term in the realization of SDEA during Voigt model rendering. Figure 6c shows that higher  $K_{ref}$  slightly improves the virtual stiffness rendering, while slightly reducing the virtual damping fidelity due to the decreased  $\sigma(B_m + G_m)$  term for higher  $K_{ref}$  values. Similarly, Figure 6d indicates that increasing  $B_{ref}$  broadens the range of virtual damping due to the lower inerter term. As the the damping of the physical filter dictates the high-frequency dynamics, all Bode plots converge to this damping.

Insight into the disturbance rejection performance of SDEA during Voigt model rendering can also be gained through physical realizations. In particular, if we consider a disturbance torque  $F_{dist}$  acting on the system at the same location with the actuator input in Figure 1, the disturbance response of the closed-loop SDEA system under VSIC with P-P controllers during Voigt model rendering can be derived as

$$Y_{fVoigt}^{SDEA^{P-P}}(s) = \frac{\omega_{end}}{F_{dist}} \bigg|_{\tau_{sea}=0} = \frac{s}{J_m s^2 + (B_m + G_m + B_{ref}\alpha)s + \alpha K_{ref}} \quad (25)$$

The disturbance transfer function  $Y_{fVoigt}^{SDEA^{P-P}}$  in Eqn. (25) is in the form of a passive admittance of an inerter  $J_m$ , damper  $(B_m + G_m + B_{ref}\alpha)$  and spring  $\alpha K_{ref}$  in parallel; hence,  $Y_{fVoigt}^{SDEA^{P-P}}$  decreases with larger controller gains and  $K_{ref}$ , indicating better disturbance attenuation. The physical realization of  $Y_{fVoigt}^{SDEA^{P-P}}$  emphasizes the effect of  $\alpha K_{ref}$  as the restoring spring that counteracts disturbances.

Please note that the disturbance responses for the linear

spring and null impedance rendering cases are recovered when  $B_{ref} = 0$  and  $K_{ref} = B_{ref} = 0$ , respectively.

**SEA:** Figure 7a indicates that an increase in  $G_t$  results in a wider frequency range for successful virtual stiffness rendering, while decreasing the virtual damping range, due to lower  $c_{2v}$  values. Figure 6b suggests that the changes in  $G_m$  have a minimal effect on spring rendering, but lower  $G_m$  values increase the range of virtual damping. Figure 7c shows that the range of virtual stiffness becomes higher with larger  $K_{ref}$ , but virtual damping displays a reduced range at the intermediate frequencies for higher  $K_{ref}$  values. Since high  $K_{ref}$  values make  $c_{1v}$  more decoupled from the system, pure damping cannot be effectively rendered at intermediate frequencies. Figure 7d shows that the virtual damping can be controlled by different selections of  $B_{ref}$  values. A selection of lower  $B_{ref}$  slightly increases the range of virtual stiffness, but slightly reduces the range of virtual damping. As the stiffness of the physical filter dictates the high-frequency dynamics, all plots converge to this stiffness.

If we consider a disturbance torque  $F_{dist}$  acting on the system at the same location with the actuator input in Figure 1, the disturbance response  $Y_{fVoigt}^{SEA^{P-P}}(s)$  of the closed-loop SEA system under VSIC with P-P controllers during spring rendering is identical to that of SDEA given in Eqn. (25). Hence, the addition of  $B_f$  does not affect this disturbance response.

### D. Effects of Filter Parameters on Voigt Model Rendering

Figure 8a shows that lowering  $B_f$  increases the range of virtual stiffness for SDEA, while the accuracy of virtual stiffness decreases. Moreover, lowering  $B_f$  decreases the range of virtual damping as it results in higher  $b_{1v}$ . Figure 8b shows that lowering  $K$  increases the range of the virtual stiffness, while it has a minimal effect on the virtual damping. The



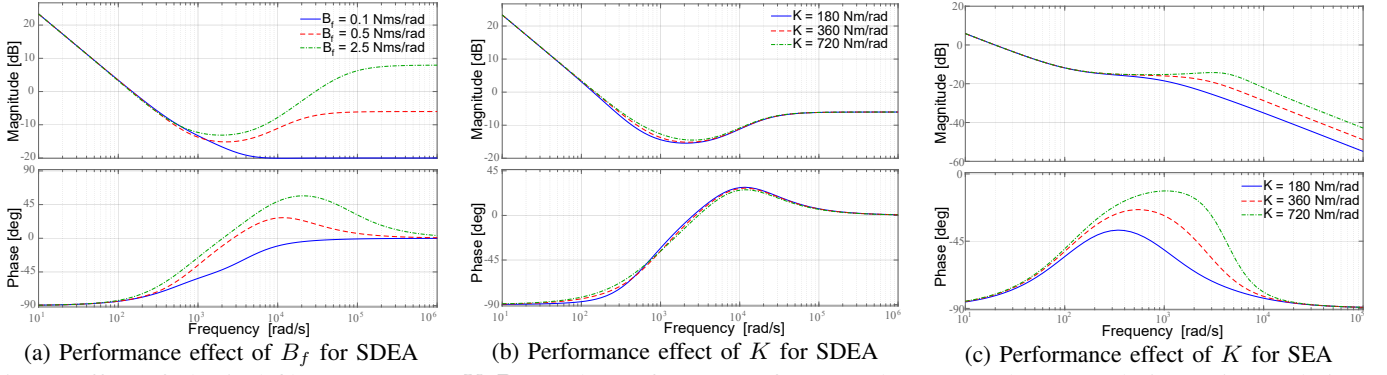


Fig. 8: Effect of physical filter parameters  $K$ - $B_f$  on the performance of SEA and SDEA under VSIC during Voigt rendering

plant damping is scaled with  $\sigma$ , which gets lower with lower  $K$ , resulting in higher performance in the low frequency range.

Figure 8c shows that increasing  $K$  has a minimal effect on the range of virtual stiffness for SEA, while it increases the range of virtual damping. Increasing  $K$  has the same effect as lowering  $K_{ref}$ , since they increase  $K - \frac{\alpha}{\alpha+1} K_{ref}$  making  $c_{2v}$  and  $c_{3v}$  more coupled from the rest of the system.

#### E. Effects of Plant Parameters on Voigt Model Rendering

Up to the control bandwidth, utilizing a plant with lower  $J_m$  has the same effect as employing higher  $G_m$  for SEA and SDEA. Figures 9a and 9c show that lowering  $J_m$  has minimal effect on the spring rendering performance, but increases the range of virtual damping, similar to using a higher  $G_m$  for SDEA. Higher  $J_m$  increases range of the virtual damping for SEA, similar to using a lower  $G_m$  for SEA. Figure 9d shows that lowering  $B_m$  increases the range of virtual stiffness and damping, similar to utilizing a higher  $G_t$  for SDEA. Figure 9b shows that lowering  $B_m$  increases the range of virtual stiffness, while decreasing the range of virtual damping, similar to utilizing a higher  $G_t$  for SEA.

## VI. CO-DESIGN AND COMPARISON OF SEA VS SDEA

### A. Co-Design via Passive Physical Equivalents

The physical plant parameters are crucial as they determine the limits of haptic rendering performance under passivity constraints [8], [9], [30]. When the causal controllers roll-off, the dynamics of the uncontrolled plant are recovered for all closed-loop systems. Accordingly, when the controller gains are set to zero in the realizations, SEA acts as a physical spring  $K$ , while an SDEA acts as a physical spring-damper  $K$ - $B_f$  pair at high frequencies as seen from the interaction port.

Given passive physical equivalents do not distinguish between the plant parameters and the controller gains, they promote co-design thinking by enforcing simultaneous and unbiased consideration of controller and plant dynamics on the closed-loop system performance [30], [62], [63]. For instance, in terms of rendering fidelity, the passive physical equivalents of SEA and SDEA under VSIC while rendering Voigt, linear spring, and null impedance models indicate that the selection of higher controller gains has the same effects as employing a plant with lower inertia and damping, as the controllers

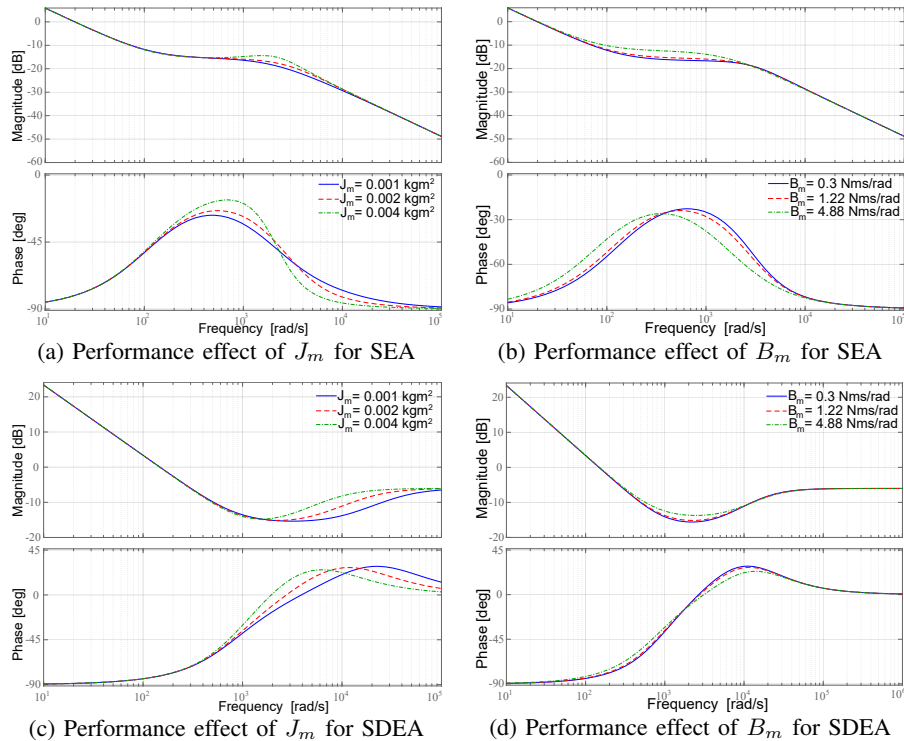


Fig. 9: Effect of plant parameters  $J_m$ - $B_m$  on the performance of SEA and SDEA under VSIC during Voigt model rendering



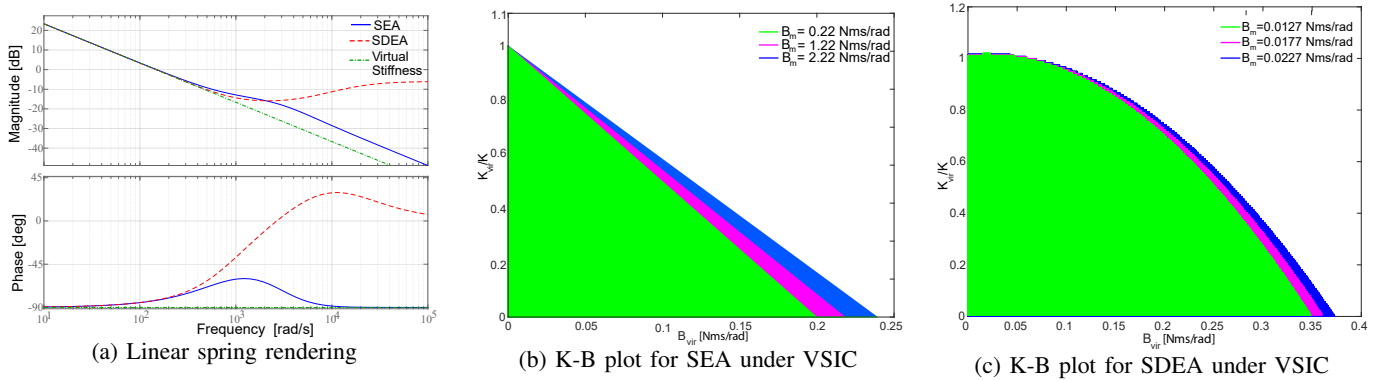


Fig. 10: Spring rendering performance and K-B plot comparison during Voigt model rendering between S(D)EA under VSIC

can compensate for the plant dynamics up to their control bandwidth. On the other hand, lower inertia and damping parameters of the plant necessitate lower controller gains to ensure passivity.

Since the plant damping is commonly considered as a parasitic effect, passive Voigt model rendering with SEA has gone unnoticed in the literature, until this study, where passive realizations are considered for the analysis. A close inspection of the passive physical equivalent of SEA during Voigt model rendering presented in Table Ie indicates that higher virtual damping  $B_{vir}$  levels can be passively rendered if  $c_{2v}$  can be set high. The upper bound of  $c_{2v}$  is imposed by  $\frac{B_m + G_m}{(\alpha + 1)}$ , as  $B_{ref}$  needs to be negative for the passivity. Hence, if the upper bound on passive damping rendering is to be increased, then one can employ a plant with higher  $B_m$ . This motivates the intentional addition of electrical damping to the system to augment the motor damping; a method commonly employed for sampled-data passivity of impedance-type haptic interfaces [64]. Utilizing a plant with higher  $B_m$  not only enables the passive rendering of higher virtual damping but also relaxes the bounds on the virtual stiffness, enlarging the  $K_{vir}$ - $B_{vir}$  plot, as depicted in Figure 10b. Furthermore, since the rendered damping becomes more coupled to the interaction port as the stiffness of the filter gets higher, one can increase  $K$  to improve the damping rendering performance.

### B. Rendering Performance Comparison of SEA vs SDEA

For spring rendering, the realizations in Table Ic and If indicate that both SEA and SDEA include identical parasitic damper terms, while their parasitic inerter terms differ. Furthermore, SDEA includes an extra branch with frequency-dependent damping effect that increases with the frequency. Figure 10a presents a comparison of the linear spring rendering performance of SEA and SDEA when the controller gains are selected to be the same. Figure 10a indicates that the performance of SEA and SDEA are close to each other in the low frequency range, while the transition from spring rendering to high frequency dynamics differs significantly.

For Voigt model rendering, the realizations in Table Ib and Ie for SEA and SDEA under VSIC have distinct topologies, as they are valid for non-overlapping parameter ranges. The  $K_{vir}$ - $B_{vir}$  plot for SEA is depicted in Figure 10b, where the boundaries of the plot are  $\frac{\alpha}{\alpha+1} K_{ref}$  and  $\frac{\alpha}{\alpha+1} B_{ref}$ , respectively. Figure 10b indicates that the selection of higher  $B_{ref}$  values allows for passive rendering of lower  $K_{vir}$  levels.

The  $K_{vir}$ - $B_{vir}$  plot of SDEA under VSIC during Voigt model rendering is presented in the Figure 10c, for the case when the system parameters are such that Condition (iv) of Theorem 2 is more conservative, as is the case for the experimental setup in Section VII. Alternatively, if the system parameters are such that Condition (i) of Theorem 2 is the more conservative, then  $K_{vir}$  increases with higher  $B_{vir}$  as presented in the Supplementary Document [61].

## VII. EXPERIMENTAL VALIDATION

In this section, we experimentally validate the theoretical passivity bounds and the haptic rendering performance of S(D)EA using a customized version of the single degree of freedom series elastic brake pedal presented in [65], [66]. The series elastic brake pedal, presented in the Multimedia Extension, is actuated by a brushless DC motor equipped with a Hall-effect sensor and an optical encoder. The torque output of the motor is amplified with a gearbox and a capstan reduction featuring 1:10 and 1:3.95 transmission ratios, respectively. The series elastic element is implemented as a linear spring through a compliant cross-flexure joint embedded into the capstan pulley. The deflections of the cross-flexure joint are measured with a linear encoder to estimate the interaction torques. All controllers are implemented in real-time at 1 kHz utilizing an industrial PC connected to an EtherCAT bus.

To implement a series *damped* elastic brake pedal, linear eddy current damping is added in parallel to the compliant element of the SEA brake pedal. In particular, permanent magnets arranged as a Halbach array to augment the magnetic field are placed to face an aluminum plate. The distance between the magnet array and aluminum plate is adjusted to control the viscous damping added to the system. When the magnets are removed, the SDEA pedal simplifies to an SEA.

### A. Identification of Plant Parameters

An accurate determination of the plant parameters is important to verify the passivity bounds of the system. First, the stiffness and damping of the physical filter are identified.

The stiffness of the cross-flexure joint is experimentally determined by applying pre-determined torques to the end-effector and measuring the resulting deflections when the actuator is locked. A least square fit to the experimental data indicates that  $K = 121.8$  N-m/rad with  $R^2 = 0.99$ .

For the identification of the damping coefficient, the magnet array is fixed to a force sensor and the motion of the aluminum plate is controlled to follow a reference chirp signal with an

amplitude of 33.5 rad/sec over the range of 0.9-1.4 Hz. A least square fit to the experimental data indicates that  $B_f = 0.0127$  N-m s/rad with  $R^2 = 0.84$ .

Closed-loop system identification is utilized to experimentally determine the system parameters related to the motor and the power transmission. The closed-loop identification enables accurate prediction of the plant parameters using LTI techniques since the robust motion controller effectively compensates for the hard-to-model nonlinear effects in the power transmission. To determine the reflected inertia and damping of the plant, the system identification is performed under the inner velocity controller with  $G_m = 0.0576$  N-m s/rad. A chirp velocity reference signal with an amplitude of 7.85 rad/sec is applied to the motion control loop over the range of 0.001-10 Hz, while no exogenous torque  $\tau_{sea}$  is applied to the system. A first-order transfer function is fitted to the data to determine the plant parameters as  $J_m = 0.0024$  kg-m<sup>2</sup> and  $B_m = 0.0177$  N-m s/rad with  $R^2 = 0.88$ .

Please note that, for simplicity of presentation, the theoretical passivity bounds in the previous sections have been derived under the non-limiting assumption that the power transmission of the system has a unity reduction ratio. Equivalent plant parameters and controller gains can be established for systems with a reduction ratio of  $n$  by introducing the following mappings:  $J_{meq} = n^2 J_m$ ,  $B_{meq} = n^2 B_m$ , and  $G_{meq} = n^2 G_m$ , and  $G_{teq} = 1/n G_t$ . Unless otherwise stated, the controller gains of VSIC are set to  $G_m = 0.0576$  N-m s/rad and  $G_t = 25$  rad/(s N-m), respectively.

### B. Verification of Passivity Bounds

The challenging nature of the experimental determination of closed-loop system phase with high accuracy and repeatability

renders the empirical verification of system passivity through Bode phase plots unreliable. On the other hand, it has been established in the literature that the passivity of a system can also be investigated by studying the coupled stability of interactions when the system is exposed to most destabilizing environments [67]. In particular, passivity can be concluded if and only if there exists no set of ideal springs or inertias that destabilize the system under excitations that span the whole frequency spectrum [22]. For SEA, inertial environments have been determined to be among the most destabilizing [68].

To validate the theoretical passivity bounds established in this paper, the S(D)EA brake pedal is coupled to a range of inertias and impacts are imposed to the end-effector to excite the system at all possible frequencies. If the violation of coupled stability (e.g., chatter) is observed, then the system is not passive. If no violation of the coupled stability is observed after many trials during which the end-effector inertia of the S(D)EA brake pedal is gradually increased, then it is concluded that the experimental evidence indicates the passivity of the system. A video of the coupled stability experiments is provided in the Multimedia Extension.

**Voigt Model Rendering with SDEA:** In this experiment, we have investigated the coupled stability of SDEA under VSIC during Voigt model rendering when the controllers are P. To validate with the necessary and sufficient conditions provided in Theorem 2, we have tested various  $K_{ref}$  and  $B_{ref}$  values.

Figure 11a depicts the  $K_{vir}$ - $B_{ref}$  plot obtained from the experiments conducted on the brake pedal with SDEA under VSIC during Voigt rendering, where  $K_{vir} = \frac{\alpha}{\alpha+1} K_{ref}$ . The magenta and blue lines in the figure represent the theoretical passivity bound according to Conditions (i) and (v) of

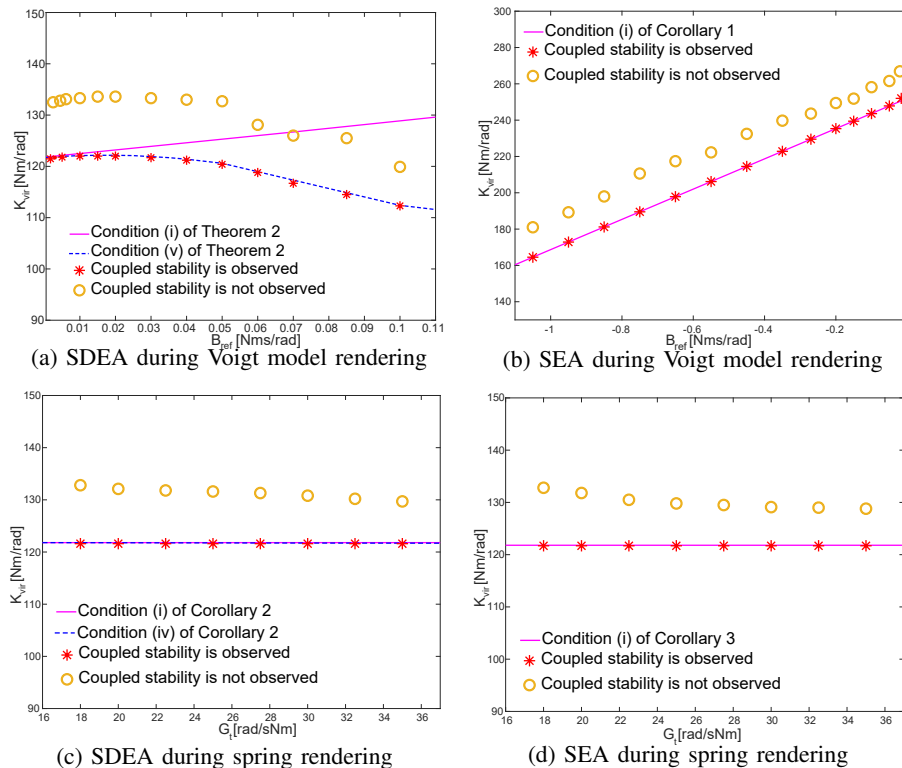


Fig. 11: Passivity bounds vs experimental coupled stability for SDEA/SEA during Voigt model and spring rendering

Theorem 2, respectively. The symbols “\*” and “o” indicate the experiments where coupled stability was preserved and compromised, respectively. The experimental results confirm the analytically predicted passivity boundaries. The experimental values are in good agreement with the theoretical values, with an error of approximately 8%. The experimental results are expected to be slightly more conservative due to unmodelled friction and hysteresis effects, which may cause extra dissipation.

**Voigt Model Rendering with SEA:** In this experiment, we have investigated the coupled stability of SEA under VSIC during Voigt model rendering when the controllers are P. To validate with the necessary and sufficient conditions provided in Corollary 1, we have tested various  $K_{ref}$  and  $B_{ref}$  values when  $G_t = 15$  rad/(s N-m).

Figure 11b depicts the  $K_{vir}-B_{ref}$  plot obtained from the experiments conducted on the brake pedal with SEA under VSIC during Voigt model rendering. In the figure, the theoretical passivity bound according to Condition (i) Corollary 1 is depicted as the magenta line. The experimental results validate the analytically predicted passivity boundary and the theoretical bound is determined to be 7% more conservative.

**Spring Rendering with SDEA:** In these experiments, we have studied the coupled stability of SDEA under VSIC during spring rendering when both controllers are P. We have selected one passive and one active  $K_{ref}$  values for eight distinct  $G_t$  gains according to the necessary and sufficient conditions given in Conditions (i) and (iv) Corollary 2.

Figure 11c presents the experimental  $K_{vir}-G_t$  plot for the SDEA brake pedal. In the figure, the theoretical passivity bound according to Condition (i) Corollary 2 is depicted as the magenta line and equal to physical stiffness of the SDEA, while the bound according to Condition (iv) Corollary 2 is depicted as the blue line. Figure 11c shows that the two conditions are very close to each other for the parameters of the SDEA brake pedal. The experimental results validate the analytically predicted passivity boundary and the theoretical bound is determined to be about 6.5% more conservative.

**Spring Rendering with SEA:** In these experiments, we have studied the coupled stability of SEA under VSIC during spring rendering when both controllers are P. We have selected one passive and one active  $K_{ref}$  values for eight distinct  $G_t$  gains

according to the necessary and sufficient condition given in Condition (i) of Corollary 3.

Figure 11d presents the experimental  $K_{vir}-G_t$  plot for the SEA brake pedal. In the figure, the theoretical passivity boundary is depicted as the magenta line and equal to physical stiffness of the SEA according to Condition (i) of Corollary 3. The experimental results validate the analytically predicted passivity boundary and the theoretical bound is determined to be about 7% more conservative.

**Null Impedance Rendering with SDEA and SEA:** In these experiments, the coupled stability of S(D)EA under VSIC during null impedance rendering when the controllers are proportional has been studied. According to the theoretical bounds, S(D)EA during null impedance rendering is passive for a wide range of positive  $G_t$  as established in Conditions (i)–(ii) of Corollaries 4 and 5. Our experiments validate this result by displaying coupled stability of interactions for a wide range of  $G_t$  gains. Conditions (i)–(ii) of Corollaries 4 and 5 are also verified for negative gains and Multimedia Extension provides sample videos of the coupled stability experiments with negative and positive gains.

### C. Evaluation of Haptic Rendering Fidelity

In this subsection, we have experimentally evaluated the performance of S(D)EA under VSIC during rendering Voigt, spring, and null impedance models. Since the haptic rendering performance of SDEA under VSIC is very similar to that of SEA for the experimental setup, only the results for SEA are provided for the brevity of the presentation.

**Null Impedance Rendering with SEA:** The performance of SEA under VSIC during null impedance rendering is important, as this control mode provides active backdrivability to allow users to move the system without much resistance.

Figure 12a presents the null impedance rendering performance of SEA under VSIC for three distinct levels of the torque controller gain  $G_t$ . As the torque controller gain  $G_t$  is increased from 20 rad/(s N-m) to 30 rad/(s N-m), the torque required to move the pedal decreases from 1.48% to 0.62% of 40 N-m torque output capacity of the SEA brake pedal. Note that this level of active-backdrivability is excellent for the SEA brake pedal, as evidenced by a commonly employed chip test (please refer to the Multi-Media Extension), where a potato

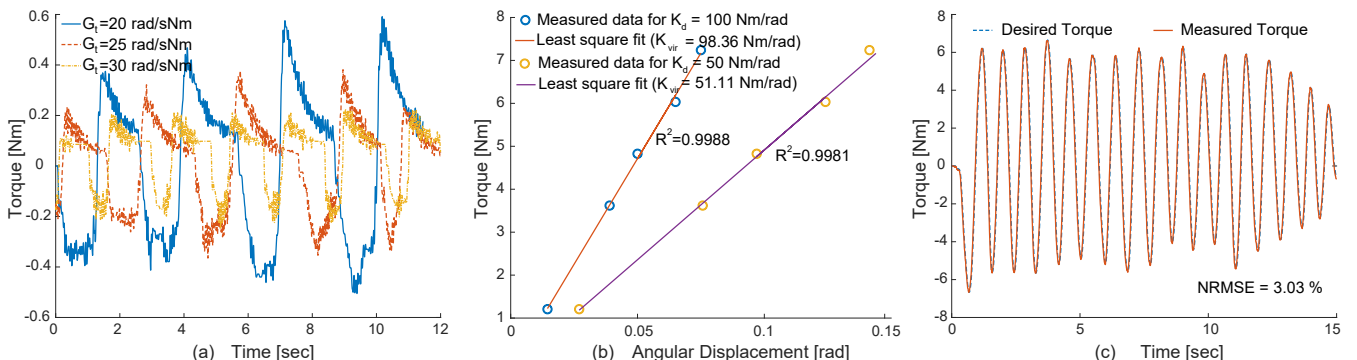


Fig. 12: (a) Null impedance rendering performance (potato chip) test for  $G_t = 20, 25$  and  $30$  rad/(s N-m), (b) Virtual stiffness rendering for  $K_{ref} = 50$  and  $100$  N-m/rad when  $G_t = 30$  rad/(s N-m), and (c) Tracking performance of SEA during virtual spring rendering with  $K_{ref} = 100$  N-m/rad and  $G_t = 30$  rad/(s N-m).

chip is used to move the device without getting broken. The experimental results in Figure 12a are also in good agreement with the analysis presented in Section V, where the positive effect of increasing the torque controller gain  $G_t$  on the null impedance rendering performance has been shown.

**Spring Rendering with SEA:** The performance of SEA under VSIC during spring rendering is important, as this control mode is commonly used to implement virtual constraints to avoid users to reach the undesired regions of the workspace. Figure 12b presents the experimental verification of the spring rendering performance for two distinct levels of virtual stiffness, where  $K_{ref} = 50$  and  $100$  N-m/rad when  $G_t = 30$  rad/(s N-m). The rendered stiffness of the SEA under VSIC is experimentally determined by applying pre-determined torques to the end-effector and measuring the resulting deflections. A least square fit to the experimental data indicates that  $K_{vir} = 51.11$  N-m/rad with  $R^2 = 0.99$  and  $K_{vir} = 98.36$  N-m/rad with  $R^2 = 0.99$ , resulting in 3.73% error for  $K_{ref} = 50$  N-m/rad and 0.19% error for  $K_{ref} = 100$  N-m/rad, respectively. These experiments are repeated for  $G_t = 25$  rad/(s N-m). In this case, a least square fit to the experimental data indicates that  $K_{vir} = 51.27$  N-m/rad with  $R^2 = 0.99$  and  $K_{vir} = 98.99$  N-m/rad with  $R^2 = 0.99$ , resulting in 4.35% error for  $K_{ref} = 50$  N-m/rad and 0.73% error for  $K_{ref} = 100$  N-m/rad, respectively. The experimental results in Figure 12b are in good agreement with the analysis presented in Section V, where the positive effects of increasing the torque controller gain  $G_t$  and desired virtual stiffness  $K_{ref}$  on the spring rendering performance have been shown.

Figure 12c presents the interaction performance of the SEA brake pedal under dynamic inputs from a user. During these experiments, the SEA brake pedal was rendering a virtual stiffness of  $K_{ref} = 50$  N-m/rad with  $G_t = 30$  rad/(s N-m). The desired interaction torque due to the virtual stiffness model and the interaction torques estimated through the series elastic element are presented with dashed and solid lines, respectively. The normalized RMS error for this dynamic tracking task is computed as 3.03%. This experiment was also repeated for  $G_t = 25$  rad/(s N-m). In this case, the normalized RMS error is computed as 3.28%. These experimental results are in good agreement with the analysis presented in Section V, where it has been demonstrated that increasing the torque controller gain  $G_t$  improves the force tracking performance.

**Voigt Model Rendering with S(D)EA:** The interaction performance of the brake pedal under dynamic inputs from a user is studied for SDEA during Voigt model rendering. The interaction performance is experimentally verified while SDEA brake pedal is rendering a Voigt model with  $K_{ref} = 100$  Nm/rad and  $B_{vir} = 0.01$  Nms/rad. The desired interaction torque due to the virtual Voigt model is computed and compared with the interaction torques estimated through the series damped elastic element. These experimental results indicate a normalized RMSE of 1.3%, validating the fidelity of the Voigt model rendering task with SDEA.

A similar experiment has also been conducted for the experimental verification of the interaction performance of the SEA brake pedal under dynamic inputs from a user while

rendering a Voigt model with  $K_{ref} = 100$  Nm/rad and  $B_{vir} = 0.01$  Nms/rad. The normalized RMSE is computed as 4.3%, indicating high fidelity for the Voigt model rendering task.

## VIII. CONCLUSIONS AND DISCUSSION

We have presented the passivity analysis of SEA and SDEA under VSIC while rendering Voigt models, linear springs, and the null impedance, and provided the necessary and sufficient conditions for the passivity of these systems. Our results significantly extend the results on S(D)EA passivity in the literature [22], [28], [29], by providing the necessity of the conditions and allowing the controller gains to be negative, and enabling passive Voigt model rendering with SEA under VSIC.

In addition to the passivity analyses, we have derived minimal passive mechanical equivalents for these systems to provide intuition into their closed-loop dynamics. The passive mechanical equivalents make the control authority and parasitic dynamics of the system explicit and enable the rigorous study of system parameters and controller gains on the rendering performance. The passive mechanical equivalents provide a concrete understanding of the limitations of rendering performance (e.g., the stiffness of the physical stiffness provides an upper bound on virtual spring rendering under VSIC). Note that these results significantly extend the interaction control analyses in [9], [30] to S(D)EA and provide insights into the robust stability-transparency trade-off of S(D)EA.

We have also demonstrated that passive mechanical equivalents enable fair comparisons of different plants (e.g., SEA vs SDEA) on the haptic rendering performance. Unlike the case in numerical studies, comparisons of closed-loop system dynamics through passive physical equivalents are informative in that these conclusions can be generalized. These comparisons highlight the impact of different plant and controller terms on the closed-loop rendering performance. Furthermore, since there exists continuity among realizations, the effect of each controller term on plant dynamics can be rigorously studied. Moreover, these comparisons are symbolic in nature and do not require performance optimization of each closed-loop system to ensure fairness, as emphasized in [57].

We have also emphasized that passive mechanical equivalents provide a physical realization of the effective impedance, establishing an intuitive understanding of the effective impedance analysis. For instance, realizations show how a frequency-dependent damping effect in the effective impedance analysis can be realized with a serial connection of an inerter with a damper, as in [52].

We have advocated that passive physical equivalents promote co-design by enabling concurrent consideration of plant parameters and controller gains on the haptic rendering performance. The realization of Voigt model rendering with SEA is provided as an illustrative example that demonstrates how the plant damping can be augmented and negative controller gains can be employed to achieve a larger range of passively renderable virtual environments.

It is important to note that, in general, passive physical realizations for a given impedance transfer function are not unique. While the feasibility conditions for a passive physical realization provide sufficient conditions for passivity as shown



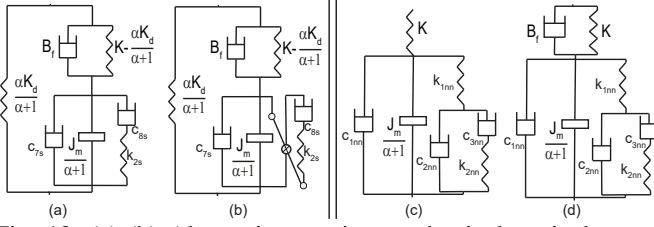


Fig. 13: (a)-(b) Alternative passive mechanical equivalents of SDEA under VSIC during spring rendering when controllers are P, and (c)-(d) Realization of S(D)EA under VSIC during null impedance rendering when controllers are PI.

in Section IV, the necessity cannot be easily established through such analysis, as it requires studying the feasibility of *all* passive physical realizations.

Figures 13a–b depict alternative passive mechanical equivalents for the impedance in Eqn. (16) for SDEA under VSIC during spring rendering when both controllers are P. Here, Figures 13a and 13b complement each other to provide the same sufficient conditions as presented for Table Ih. While Bott-Duffin theorem [35] establishes that ideal transformers (levers) can be avoided in non-minimal physical realizations, we present Figures 13a and 13b as a set of alternative minimal realizations, since we prioritize minimality of the realizations, the feasibility conditions of these two realizations complement each other to recover the necessary and sufficient conditions for the passivity of Eqn. (16), and the use of a lever to change direction provides an understanding on how negative values of fundamental elements (e.g.,  $k_{1n}$  and  $c_{4n}$ ) can be avoided.

Realizations become more complicated as controllers become more involved, making their interpretation harder. For instance, Figures 13c–d present passive physical realizations for SEA and SDEA under VSIC during null impedance rendering, when both controllers are PI. As the realizations become more complicated, the feasibility conditions for the realizations are likely to cover a smaller range of passive system parameters; hence, conclusions drawn from such realizations become valid for a limited range. Accordingly, it is preferable to utilize the simplest models competent to represent the essential dynamic behavior, as recommended in [30].

This study utilizes classical analysis techniques to derive closed-form analytical solutions for the passivity bounds of LTI systems in the frequency domain. There exist alternative approaches for passivity analysis, for instance utilizing state-space techniques, for which equivalences with the frequency domain analysis have been established [58]. Moreover, less conservative analysis techniques, such as time domain passivity [69] or complementary stability [56], [57], [70] can be applied, if numerical approaches are to be utilized.

Our ongoing work includes the extension of the passivity analysis and realization results to S(D)EA under different controllers, such as MRFC [26]. We also plan to extend passive realizations to fractional-order LTI systems [54], [55], as these controllers can benefit from physical intuition.

As part of our future work, we plan to study extensions of the current results to S(D)EA systems that include non-linear energy storage and dissipation elements, utilizing well-established passivity definitions and analysis techniques for nonlinear and infinite dimensional systems [71], [72].

## ACKNOWLEDGMENTS

This work has been partially supported under TÜBİTAK Grants 216M200 and 23AG003.

## REFERENCES

- [1] N. Hogan, “Impedance control: An approach to manipulation: Part I—Theory,” *J. of Dynamic Systems, Measurement, and Control*, vol. 107, no. 1, pp. 1–7, 1985.
- [2] J. E. Colgate and N. Hogan, “Robust control of dynamically interacting systems,” *Int. Journal of Control*, vol. 48, no. 1, pp. 65–88, 1988.
- [3] R. D. Howard, “Joint and actuator design for enhanced stability in robotic force control,” Ph.D. dissertation, MIT, 1990.
- [4] G. A. Pratt and M. M. Williamson, “Series elastic actuators,” in *IEEE/RSJ Int. Conf. on Intel. Rob. and Sys.*, vol. 1, 1995, pp. 399–406.
- [5] D. W. Robinson, J. E. Pratt, D. J. Paluska, and G. A. Pratt, “Series elastic actuator development for a biomimetic walking robot,” in *IEEE/ASME Int. Conf. on Adv. Intel. Mech.*, 1999, pp. 561–568.
- [6] C. An and J. Hollerbach, “Dynamic stability issues in force control of manipulators,” in *IEEE Int. Conf. on Rob. and Auto.*, vol. 4, 1987, pp. 890–896.
- [7] S. Eppinger and W. Seering, “Understanding bandwidth limitations in robot force control,” in *IEEE Int. Conf. on Rob. and Auto.*, vol. 4, 1987, pp. 904–909.
- [8] W. S. Newman, “Stability and performance limits of interaction controllers,” *J. of Dynamic Sys., Meas., and Cont.*, vol. 114, no. 4, pp. 563–570, 1992.
- [9] C. U. Kenanoglu and V. Patoglu, “A fundamental limitation of passive spring rendering with series elastic actuation,” *IEEE Trans. on Haptics*, 2023, online first.
- [10] J. Hurst, A. Rizzi, and D. Hobbelen, “Series elastic actuation: Potential and pitfalls,” in *Int. Conf. on Climbing and Walking Rob.*, 2004.
- [11] J. Oblak and Z. Matjačić, “Design of a series visco-elastic actuator for multi-purpose rehabilitation haptic device,” *J. of Neuroeng. and Rehab.*, vol. 8, no. 1, pp. 1–14, 2011.
- [12] E. Garcia, J. C. Arevalo, G. Muñoz, and P. Gonzalez-de Santos, “Combining series elastic actuation and magneto-rheological damping for the control of agile locomotion,” *Rob. and Auto. Sys.*, vol. 59, no. 10, pp. 827–839, 2011.
- [13] M. Laffranchi, N. Tsagarakis, and D. G. Caldwell, “A compact compliant actuator (compact) with variable physical damping,” in *IEEE Inter. Conf. on Rob. and Auto.*, 2011, pp. 4644–4650.
- [14] M. J. Kim, A. Werner, F. C. Loeffl, and C. Ott, “Enhancing joint torque control of series elastic actuators with physical damping,” in *IEEE Int. Conf. on Rob. and Auto.*, 2017, pp. 1227–1234.
- [15] G. Pratt, P. Willisson, C. Bolton, and A. Hofman, “Late motor processing in low-impedance robots: impedance control of series-elastic actuators,” in *American Control Conference*, 2004, pp. 3245–3251.
- [16] G. Wyeth, “Control issues for velocity sourced series elastic actuators,” in *Australasian Conf. on Rob. and Auto.*, 2006, pp. 1–6.
- [17] —, “Demonstrating the safety and performance of a velocity sourced series elastic actuator,” in *IEEE Inter. Conf. on Rob. and Auto.*, 2008, pp. 3642–3647.
- [18] H. Vallery, R. Ekkelenkamp, H. Van Der Kooij, and M. Buss, “Passive and accurate torque control of series elastic actuators,” in *IEEE/RSJ Int. Conf. on Intel. Rob. and Sys.*, 2007, pp. 3534–3538.
- [19] H. Vallery, J. Veneman, E. Van Asseldonk, R. Ekkelenkamp, M. Buss, and H. Van Der Kooij, “Compliant actuation of rehabilitation robots,” *IEEE Rob. and Auto. Mag.*, vol. 15, no. 3, pp. 60–69, 2008.
- [20] N. L. Tagliamonte and D. Accoto, “Passivity constraints for the impedance control of series elastic actuators,” *Inst. of Mech. Eng., Part I: J. of Sys. and Cont. Eng.*, vol. 228, no. 3, pp. 138–153, 2014.
- [21] A. Calanca, R. Muradore, and P. Fiorini, “Impedance control of series elastic actuators: Passivity and acceleration-based control,” *Mechatronics*, vol. 47, pp. 37–48, 2017.
- [22] F. E. Tosun and V. Patoglu, “Necessary and sufficient conditions for the passivity of impedance rendering with velocity-sourced series elastic actuation,” *IEEE Trans. on Robotics*, vol. 36, no. 3, pp. 757–772, 2020.
- [23] O. T. Kenanoglu, C. U. Kenanoglu, and V. Patoglu, “Effect of low-pass filtering on passivity and rendering performance of series elastic actuation,” *IEEE Trans. on Haptics*, 2023, online first.
- [24] A. Otaran, O. Tokatli, and V. Patoglu, “Physical human-robot interaction using HandsOn-SEA: An educational robotic platform with series elastic actuation,” *IEEE Trans. on Haptics*, vol. 14, no. 4, pp. 922–929, 2021.
- [25] A. Calanca and P. Fiorini, “A rationale for acceleration feedback in force control of series elastic actuators,” *IEEE Trans. on Robotics*, vol. 34, no. 1, pp. 48–61, 2018.

- [26] C. U. Kenanoglu and V. Patoglu, "Passivity of series elastic actuation under model reference force control during null impedance rendering," *IEEE Trans. on Haptics*, vol. 15, no. 1, pp. 51–56, 2022.
- [27] M. Focchi, G. A. Medrano-Cerda, T. Boaventura, M. Frigerio, C. Semini, J. Buchli, and D. G. Caldwell, "Robot impedance control and passivity analysis with inner torque and velocity feedback loops," *Control Theory and Tech.*, vol. 14, no. 2, pp. 97–112, 2016.
- [28] U. Mengilli, U. Caliskan, Z. O. Orhan, and V. Patoglu, "Two-port analysis of stability and transparency in series damped elastic actuation," *CoRR*, 2020. [Online]. Available: <https://arxiv.org/abs/2011.00664>
- [29] U. Mengilli, Z. O. Orhan, U. Caliskan, and V. Patoglu, "Passivity of series damped elastic actuation under velocity-sourced impedance control," in *IEEE World Haptics Conf.*, 2021, pp. 379–384.
- [30] E. Colgate and N. Hogan, "An analysis of contact instability in terms of passive physical equivalents," in *Int. Conf. on Rob. and Auto.*, vol. 1, 1989, pp. 404–409.
- [31] M. C. Smith, "Synthesis of mechanical networks: the inerter," *IEEE Trans. on Automatic Control*, vol. 47, no. 10, pp. 1648–1662, 2002.
- [32] M. Z. Chen, C. Papageorgiou, F. Scheibe, F.-c. Wang, and M. C. Smith, "The missing mechanical circuit element," *IEEE Circ. and Sys. Mag.*, vol. 9, no. 1, pp. 10–26, 2009.
- [33] R. M. Foster, "A reactance theorem," *Bell System Technical Journal*, vol. 3, no. 2, pp. 259–267, 1924.
- [34] O. Brune, "Synthesis of a finite two-terminal network whose driving-point impedance is a prescribed function of frequency," Ph.D. dissertation, MIT, 1931.
- [35] R. Bott and R. Duffin, "Impedance synthesis without use of transformers," *Journal of Applied Physics*, vol. 20, no. 8, pp. 816–816, 1949.
- [36] M. Z. Chen and M. C. Smith, "Mechanical networks comprising one damper and one inerter," in *IEEE European Control Conf.*, 2007, pp. 4917–4924.
- [37] —, "Restricted complexity network realizations for passive mechanical control," *IEEE Trans. on Auto. Control*, vol. 54, no. 10, pp. 2290–2301, 2009.
- [38] M. Z. Chen, K. Wang, Y. Zou, and J. Lam, "Realization of a special class of admittances with one damper and one inerter," in *IEEE Conf. on Decision and Control*, 2012, pp. 3845–3850.
- [39] —, "Realization of a special class of admittances with one damper and one inerter for mechanical control," *IEEE Trans. on Auto. Control*, vol. 58, no. 7, pp. 1841–1846, 2013.
- [40] M. Z. Chen, K. Wang, Z. Shu, and C. Li, "Realizations of a special class of admittances with strictly lower complexity than canonical forms," *IEEE Trans. on Circ. and Sys. I*, vol. 60, no. 9, pp. 2465–2473, 2013.
- [41] M. Z. Chen, K. Wang, Y. Zou, and G. Chen, "Realization of three-port spring networks with inerter for effective mechanical control," *IEEE Trans. on Auto. Control*, vol. 60, no. 10, pp. 2722–2727, 2015.
- [42] R. Kalman, *Perspectives in Mathematical System Theory, Control, and Signal Processing*. Berlin, Heidelberg: Springer, 2010, vol. 398, ch. Old and new directions of research in system theory, p. 3.
- [43] J. Z. Jiang and M. C. Smith, "Regular positive-real functions and five-element network synthesis for electrical and mechanical networks," *IEEE Trans. on Auto. Control*, vol. 56, no. 6, pp. 1275–1290, 2011.
- [44] —, "Series-parallel six-element synthesis of biquadratic impedances," *IEEE Trans. on Circ. and Sys. I*, vol. 59, no. 11, pp. 2543–2554, 2012.
- [45] T. H. Hughes and M. C. Smith, "On the minimality and uniqueness of the bott-duffin realization procedure," *IEEE Trans. on Auto. Control*, vol. 59, no. 7, pp. 1858–1873, 2014.
- [46] T. H. Hughes, "Minimal series-parallel network realizations of bicubic impedances," *IEEE Trans. on Auto. Control*, vol. 65, no. 12, pp. 4997–5011, 2020.
- [47] A. Morelli and M. C. Smith, *Passive Network Synthesis: An Approach to Classification*. SIAM, 2019.
- [48] S. M. Hughes T.H., Morelli A., *Electrical Network Synthesis: A Survey of Recent Work*, ser. Lecture Notes in Control and Inf. Sci. Springer, 2018, ch. Emerg. App. of Contr. and Sys. Theory, pp. 281–293.
- [49] B. Hannaford, "A design framework for teleoperators with kinesthetic feedback," *IEEE Trans. on Rob. and Auto.*, vol. 5, no. 4, pp. 426–434, 1989.
- [50] K. Hashtrudi-Zaad and S. E. Salcudean, "Analysis of control architectures for teleoperation systems with impedance/admittance master and slave manipulators," *Int. J. of Rob. Res.*, vol. 20, no. 6, pp. 419–445, 2001.
- [51] J. Colgate and J. Brown, "Factors affecting the Z-width of a haptic display," in *IEEE Int. Conf. on Rob. and Auto.*, 1994, pp. 3205–3210.
- [52] J. S. Mehling, J. E. Colgate, and M. A. Peshkin, "Increasing the impedance range of a haptic display by adding electrical damping," in *IEEE World Haptics Conf.*, 2005, pp. 257–262.
- [53] N. Colonnese, A. F. Siu, C. M. Abbott, and A. M. Okamura, "Rendered and characterized closed-loop accuracy of impedance-type haptic displays," *IEEE Trans. on Haptics*, vol. 8, no. 4, pp. 434–446, 2015.
- [54] O. Tokatli and V. Patoglu, "Stability of haptic systems with fractional order controllers," in *IEEE/RSJ Int. Conf. on Intel. Rob. and Sys.*, 2015, pp. 1172–1177.
- [55] —, "Using fractional order elements for haptic rendering," *Springer Adv. Rob. Res.*, pp. 373–388, 2018.
- [56] Y. Aydin, O. Tokatli, V. Patoglu, and C. Basdogan, "Stable physical human-robot interaction using fractional order admittance control," *IEEE Trans. on Haptics*, vol. 11, no. 3, pp. 464–475, 2018.
- [57] —, "A computational multicriteria optimization approach to controller design for physical human-robot interaction," *IEEE Trans. on Robotics*, vol. 36, no. 6, pp. 1791–1804, 2020.
- [58] N. Kottenstette and P. J. Antsaklis, "Time domain and frequency domain conditions for passivity," ISIS Lab Univ. of Notre Dame, Technical report ISIS-2008-002, 2008.
- [59] S. Haykin, *Active network theory*. Addison-Wesley Pub. Co., 1970.
- [60] F. F. Kuo, *Network Analysis and Synthesis*. John Wiley and Sons, 1962.
- [61] C. U. Kenanoglu and V. Patoglu, "Supplementary document for passive realizations of series elastic actuation," Sabanci University, Tech. Rep., 2022. [Online]. Available: <https://tinyurl.com/u5f2e5ev>
- [62] A. Kamadan, G. Kiziltas, and V. Patoglu, "Co-design strategies for optimal variable stiffness actuation," *IEEE/ASME Trans. on Mech.*, vol. 22, no. 6, pp. 2768–2779, 2017.
- [63] —, "A systematic design selection methodology for system-optimal compliant actuation," *Robotica*, vol. 37, no. 4, pp. 656–674, 2019.
- [64] D. W. Weir, J. E. Colgate, and M. A. Peshkin, "Measuring and increasing z-width with active electrical damping," *Symp. on Haptic Interfaces for Virtual Environment and Teleoperator Systems*, pp. 169–175, 2008.
- [65] U. Caliskan, A. Apaydin, A. Otaran, and V. Patoglu, "A series elastic brake pedal to preserve conventional pedal feel under regenerative braking," in *IEEE/RSJ Int. Conf. on Intel. Rob. and Sys.*, 2018, pp. 1367–1373.
- [66] U. Caliskan and V. Patoglu, "Efficacy of haptic pedal feel compensation on driving with regenerative braking," *IEEE Trans. on Haptics*, vol. 13, no. 1, pp. 175–182, 2020.
- [67] J. E. Colgate, "The control of dynamically interacting systems," Ph.D. dissertation, MIT, 1988.
- [68] D. P. Losey and M. K. O'Malley, "Effects of discretization on the k-width of series elastic actuators," in *IEEE Int. Conf. on Rob. and Auto.*, 2017, pp. 421–426.
- [69] B. Hannaford and J.-H. Ryu, "Time domain passivity control of haptic interfaces," *IEEE Trans. on Rob. and Auto.*, vol. 18, no. 1, pp. 1–10, 2002.
- [70] S. P. Buerger and N. Hogan, "Complementary stability and loop shaping for improved human-robot interaction," *IEEE Trans. on Robotics*, vol. 23, no. 2, pp. 232–244, 2007.
- [71] R. Ortega, J. A. L. Perez, P. J. Nicklasson, and H. J. Sira-Ramirez, *Passivity-based control of Euler-Lagrange systems: mechanical, electrical and electromechanical applications*. Springer Science, 2013.
- [72] V. Duindam, A. Macchelli, S. Stramigioli, and H. Bruyninckx, *Modeling and control of complex physical systems: the port-Hamiltonian approach*. Springer Science, 2009.

**Celal Umur Kenanoglu** received his B.Sc. degree in mechanical engineering from Izmir Institute of Technology (2019) and his M.Sc. in mechatronics engineering from Sabanci University (2022). Currently, he is pursuing his Ph.D. in the Munich Institute of Robotics and Machine Intelligence at the Technical University of Munich. His research interests include interaction control, physical human-robot interaction, and haptic rendering.

**Volkan Patoglu** is a professor in mechatronics engineering at Sabanci University. He received his Ph.D. degree in mechanical engineering from the University of Michigan, Ann Arbor (2005) and worked as a post-doctoral research associate at Rice University (2006). His research is in the area of physical human-machine interaction, in particular, design and control of force feedback robotic systems with applications to rehabilitation. His research extends to cognitive robotics. Dr. Patoglu has served as an associate editor for IEEE Transactions on Haptics (2013–2017) and IEEE Transactions on Neural Systems and Rehabilitation Engineering (2018–2023), and is currently an associate editor for IEEE Robotics and Automation Letters.

